

Answer of Referee #1

Major comments:

1. The appeal of the originality of this study against former studies is inadequate. You should describe clearly and precisely about originality and position of this study (what is problems of former studies and how does this study solve the problems, for example) in abstract, introduction, and summary. This is most important point to correct your manuscript

Author's answer: Thank for the referee's comment. We added the originality of present study in the conclusion section as follows:

Added sentence [line 529-534]:

These results could be the essential information to develop the new approaches for detecting non-hydrometeors and numerical model. The axis ratio and canting angle of ash particles obtained from the present study are necessary for scattering simulations. V_T obtained by the present study suggests that smaller particles can be transported longer distance. Therefore, it will be useful for scattering simulation of ash particles to develop QAE and help to improve a numerical model using V_T obtained by the present study.

2. There are no description about lithological and petrographical characteristics of volcanic ash samples used in the experiment. As your manuscript show that the ranges of shapes of volcanic ash particle are wide, the contents of volcanic ash particles derived from Sakurajima Volcano are variable. For example, the tephra derived from the recent eruption of Sakurajima Volcano contains particles with various degrees of roundness, and sometimes contains tabular shaped glassy particles as co-ignimbrite ash derived from caldera forming eruption. In addition, shapes of essential glassy particles have wide variation, such as blocky and vesicular particles. Therefore, you should described classification and proportion of volcanic ash particles in the text.

Author's answer: The authors agreed with the referee's comments. However, unfortunately, the petrological characteristics of Sakurajima volcanic ash were not analyzed. Therefore we cited the recently references describing it (Oguchi et al., 2009; Takahashi et al., 2013)

Added sentence [line 252]:

~ tephra is approximately 60–66 % SiO₂ Peléan-type (Oguchi et al., 2009; Takahashi et al., 2013)

3. The introduction about characteristics of Sakurajima Volcano is insufficient in chapter 2-d.

Especially, you should described about volcanic history and characteristics of eruption type of recent eruptions from 2006 at Showa and Minamidake summit craters. The purpose is to clarify the characteristics of the volcanic ash sample used in the experiment as pointed out in above. The sampled date are described in Table 2, but there are no description about the characteristics of eruptions

Author's answer: We appreciated the referee's comments. We added the following paragraph to 2.d Sakurajima.

Added sentence [line 254-261]:

Sakurajima is an andesitic volcano with two peaks (Kita-dake and Minami-dake). Volcanic activity at Kita-dake ended around 4,900 years ago then it changed to Minami-dake. Activity has centred on Showa crater from 2006 (Iguchi, 2013). Showa crater is located on the eastern flank approximately 500 m east of Minami-dake (Southern Peak) of Sakurajima volcano. It was appeared in 1939 after one month of eruptions that year (Yokoo and Ishihara, 2007). The Minami-dake summit crater was the only active center of Sakurajima volcano until the recommencement of Showa crater from 1948 to 2006 then eruptive activity of Showa crater was resumed in June 2006 and vulcanian eruptions gradually increased in the autumn of 2009 (Hotta et al., 2016).

4. You should indicate clearly in summary about the advantage of your result and possibility about future works. The summary of first manuscript is just only description of data.

Author's answer: Thank you for the comments. A discussion section has been added to emphasize the advantage of our results.

5. Several other comments are shown in the manuscript (made by Adobe Reader).

Please also note the supplement to this comment:

<https://www.atmos-meas-tech-discuss.net/amt-2019-88/amt-2019-88-RC1-supplement.pdf>

Line 1 : "Laboratory analysis" is not most important keyword. How about "Free-fall experiment", for example.

Author's answer: 'Free-fall experiments' would be great. We will change the title.

Line 305 : Show reference.

Author's answer: This is a JMA report but, recent papers (Oguchi et al., 2009; Takahashi et al., 2013) describing the petrological characteristics of Sakurajima volcanic ash would be better for the manuscript. So, we changed the sentence.

Added sentence [line 252]:

~ tephra is approximately 60–66 % SiO₂ Peléan-type (Oguchi et al., 2009; Takahashi et al., 2013)

Line 305 : "eruptive events in historic age"

Author's answer: Thank you. We changed it.

Line 306 : Add Showa eruption and recent eruption from 2006 both at showa and Minamidake-summit craters. Furthermore, show the eruptive types of each event, and specify when the sample used in this study was taken.

Author's answer: It is judged that it is same comment for Major comment No.3.

Line 329 : "the"

Author's answer: Thank you. We changed it.

Line 612 : Specify the expected result.

Author's answer: This is future work. There are some limitations in describing the expected outcome. In addition, this study is a result obtained by 2DVD, not weather radar. Therefore, it was the authors' purpose to explain the direction of detailed research.

Answer of Referee #2

Major comments

1. As noted in the introductory part my largest issue with the manuscript is the lack of a good discussion section to put the findings into perspective. I believe there are a number of key issues concerning ash dispersal that the results are relevant to (see other points 3 and 4) and I would like to see at least some of the discussed in more detail in a larger discussion section. This doesn't have to necessarily be a separate section from the conclusions (although it would be preferred), but at least a more complete version of what was included in the first iteration. Parts of the introduction feel overly long and repetitive so I would suggest tidying up the introduction and using the space for a more comprehensive discussion section.

Author's answer: Thank for referee's comment. We have added a discussion session (section 4) to discuss in detail the future direction of research that can be expected from the results of this study. Also, we removed the sentences section that were deemed unnecessary in the introduction.

2. Speaking about the introduction, at the end it is stated that one of the two goals of the paper is to "develop QAE methods for accurate detection of ash clouds by cloud radar" (ln158-161). Although I understand that this is one of the aim of the larger study presented it is not really addressed again in the paper aside from the concluding section (ln 610-615). I feel that at this point this is future work and mainly makes sense in the conclusions; usually the last paragraph of the introduction is reserved for topics that are actually addressed in the paper.

Author's answer: The quantitative ash fall estimation (QAE) is the motivation and purpose of the present study. The authors concluded that the reasons why these variables were analyzed should be explained. The author agreed referee's comment. Therefore, all sentences related to QAE in the manuscript have been moved to the discussion section to suggest the possibility of QAE method.

3. How would ash aggregation affect the results in real conditions? Aggregation changes the new particle density and size and thus affects vertical velocity (for example see Bagheri et al 2016 Timing and nature of volcanic particle clusters based on field and numerical investigations, J. Volcanol. Geotherm. Res.). What would the effect of that be in radar observations?

Author's answer: The effects of aggregation on radar observations are outside the scope of the present study though it is important. Due to the changes in particle diameter and axial ratio through aggregation, the variation in differential reflectivity (Z_{DR}) which is a function of and the particle axial ratio and the horizontal reflectivity (Z_H) which is proportional to the sixth power of the particle diameter can be expected.

4. What would the results suggest for ash hazard simulations? How can this new knowledge be expected to impact results from volcanic ash simulations considering that volcanic ash is commonly represented as a single category with common geometry? I think that this represent an interesting point that could be touched upon to show the significance of the work.

Author's answer: The particle density and its shapes are the main factors that determine the terminal velocity. Since the particles of the oblate spheroids have a lower terminal velocity than that of the sphere. The terminal velocity of ash particle, thus, traveling distance of particles. Therefore, the higher performance of diffusion simulation results can be expected if a model considers the results of the present study.

5. Some of the paragraphs, especially in the introduction, are overly long and complicated. One paragraph should only discuss one idea, expressed by the first sentence and expanded in the following sentences. Ideally, a reader should be able to have a good idea about what is written in the paper just by reading the first sentence of each paragraph. Overly long and complicated paragraphs can be very tiring to go through.

Author's answer: Thank for the referee's comments and authors agreed the advice. Therefore, we minimized the introduction section and focused on the free-fall experiment of ash particles.

Minor and technical comments

See manuscript for minor (blue) and technical/language (green) comments. These don't have to be addressed in the response, unless the authors would like to refute them

Please also note the supplement to this comment:

<https://www.atmos-meas-tech-discuss.net/amt-2019-88/amt-2019-88-RC2-supplement.pdf>

Line 40 : I can't understand the meaning

Author's answer: Thank for the comments. We modified the sentence as follows:

Added sentence [line 40-42]:

It is interesting the terminal velocities for OH decreased rapidly in the range $0.5 < D < 1$ mm corresponding to the decrease in axis ratio (i.e., smaller the particle, the flatter the shape).

Line 42 : I would replaced with "ranged"

Author's answer: Thank for the comments. We modified the word

Line 54 : Bonadonna et al. (2011)

Author's answer: Thank you.

Line 94 : Marazano

Author's answer: Thank you.

Line 96 : > ?

Author's answer: Thank you for the comments. This is not a typo so we modified it to 'Lapilli ($D > 0.53$ mm)' based on Marzano et al. (2013).

Line 99 : can be

Author's answer: Thank you.

Line 111 : Example/reference?

Author's answer: Thank for the comments. This is information from Marzano et al. (2006). However, we removed this sentence to minimize the introduction.

Line 130 : In

Author's answer: Thank you. We removed this sentence to minimize the introduction.

Line 148 : Volcanic ash dispersal simulations?

Author's answer: This is a T-matrix scattering simulation, not a numerical model. It is described in the following paragraphs and this sentence moved to the discussion section.

Line 159 : This is future work?

Author's answer: Right. This study is the fundamental research for the development of a quantitative ash fall estimation (QAE) method based on weather radar.

Line 206 : I would rewrite to "The difference in angle between ... is defined as beta"

Author's answer: Thank you. We revised the sentence what you suggested.

Line 323 : remove the word 'by a manager'

Author's answer: Thank you.

Line 324 : This is a bit vague

Author's answer: This was cited by Maki et al. (2016) but we fully agreed to the referee's comments. Therefore, it was deleted.

Line 324 : Something seems to be missing here

Author's answer: Thank for the referee's advice. We modified 'the former data set (A, B)' to 'Type 1' to avoid confusing.

Line 331 : 2?

Author's answer: It's not a typo. The results are shown in Figure 3 of Bonadonna et al. (2011).

Line 362 : I would refer to Freret-Lorgeril et al. 2019 (J. Volcanol. Geotherm. Res.) to show a case where disdrometers were succesfully used in the field to observe ashfall

Author's answer: Thank for the referee's guidance.

Line 429 : Results are summarized..

Author's answer: Thank you.

Line 448 : This should either be expressed in $\log(\text{Re})$ to reflect the figure axis or a line should be added in the figure to indicate $\text{Re}=70$.

Author's answer: Thank for your comment. We added 'Log (Re) \sim 1.845' in line 376.

Line 546 : I feel that this section should either come after or be merged with Section b. Fig. 15 could also be added as a second panel to Fig. 9 as:

New Fig 9:

9a. Old Fig. 9

9b. Old Fig. 15

Author's answer: Thanks for the question. The authors have been concerned about the simplification of the manuscript same as the referee's opinion. We agreed the referee's advice so we removed the section 3.f and merged the figure with Fig. 9.

Line 565 : I agree with this written here but not written as a direct aim of the paper in the introduction as its future work.

Author's answer: Thank you for the comment and we agreed the referee's comment. The sentence was removed.

Fig. 8 : Number? I think this would be better expressed as a fraction.

Author's answer: Thank you. We modified as 'Fraction'.

Free-fall experiments of volcanic ash particles

using a 2D video disdrometer

Sung-Ho Suh¹ (Email: suhsh1215@pukyong.ac.kr)

Masayuki Maki^{2*} (Email: maki@gm.kagoshima-u.ac.jp)

Masato Iguchi³ (Email: iguchi@svo.dpri.kyoto-u.ac.jp)

Dong-In Lee¹ (Email: leedi@pknu.ac.kr)

Akihiko Yamaji⁴ (Email: yamaji@jwa.or.jp)

Tatsuya Momotani⁴ (Email: momotani@jwa.or.jp)

Institutional addresses:

¹Department of Environmental Atmospheric Sciences, Pukyong National University, Namgu, Busan, Republic of Korea

²Research and Education Center for Natural Hazards, Kagoshima University, Korimoto, Kagoshima, Japan

³Sakurajima Volcano Research Center, Disaster Prevention Research Institute, Kyoto University, Sakurajima, Kagoshima, Japan

⁴Japan Weather Association, Higashi-Ikebukuro, Toshima-ku, Tokyo, Japan

* Corresponding author: Masayuki Maki (maki@gm.kagoshima-u.ac.jp)

Key Points: Volcanic ash, 2DVD, aerodynamic properties, laboratory experiments

21 The English in this document has been checked by at least two professional editors, both native
22 speakers of English. For a certificate, please see:

23

24 <http://www.textcheck.com/certificate/7pU3Ux>

25

26

27 **Abstract**

28 Information of aerodynamic parameter of volcanic ash particles, such as terminal velocity, axis
29 ratio, and canting angle, which are necessary for quantitative ash-fall estimations with weather radar.
30 In this study, free-fall experiments of volcanic ash particle were accomplished using a two-dimensional
31 video disdrometer under controlled conditions.

32 Samples containing a rotating symmetric axis were selected and divided into five types according
33 to shape and orientation: oblate spheroid with horizontal rotating axis (OH), oblate spheroid with
34 vertical axis (OV), prolate spheroid with horizontal rotating axis (PH), prolate spheroid with vertical
35 rotating axis (PV), and sphere (Sp). The horizontally (OH and PH) and vertically (OV and PV) oriented
36 particles were present in proportions of 76% and 22%, and oblate and prolate spheroids were in
37 proportions of 76% and 24%, respectively. The most common shape type was OH (57%).

38 The terminal velocities of OH, OV, PH, PV and Sp were obtained analyzing 2DVD data. The
39 terminal velocities of PV were highest compared to those of other particle types. The lowest terminal
40 velocities were found in OH particles. **It is interesting the terminal velocities for OH decreased rapidly**
41 **in the range $0.5 < D < 1$ mm corresponding to the decrease in axis ratio (i.e., smaller the particle, the**
42 **flatter the shape).** The axis ratios of all particle types except Sp were found to be converged to 0.94 at
43 $D > 2$ mm.

44 The histogram of canting angles followed unimodal and bimodal distributions with respect to
45 horizontally and vertically oriented particles, respectively. The mean values and the standard deviation
46 of entire particle shape types were close to 0° and 10° , respectively under calm atmospheric conditions.

1. Introduction

Volcanic eruptions are considered one of the most severe types of natural phenomena, and can lead to human casualties and property damage. Ash consists of very fine-grained fragments, volume-equivalent spherical particle diameter (D in μm) is generally smaller than 2 mm, and these are generally dominated by broken glass shards rather than crystal and lithic fragments. Wilson et al. (2012) overview for the ash effects on critical infrastructures such as ash fall and acid rain. Hilman et al. (2012) investigate the effect ash particles on human health in case of Sakurajima volcanic eruptions. More comprehensive descriptions on the volcanic ash impacts on society is found in Sigurdsson et al. (2015) and Wilson et al. (2015). Following an eruption, fine airborne volcanic ash flows for several tens of kilometers, which can cause major problems by increasing aviation traffic (e.g., Bonadonna et al., 2012; Langmann et al., 2012); this was seen after the eruption of Eyjafjallajökull volcano in Iceland during the period April 14–21, 2010, for example Bonadonna et al. (2011). From the viewpoint of volcanological hazard reduction, accurate description of transport and deposition in the numerical forecasting model of volcanic ash clouds are vitally important (Poulidis et al., 2017).

Terminal fall velocity (V_T) of a particle is affected by its shape, density, size, and atmospheric properties. Wilson and Huang (1979), Dellino (2005), and Coltelli et al. (2008) introduced the influence of ash particle shapes on its V_T . Haider and Levenspile (1989) and Ganser (1993) analyzed V_T of volcanic ash particle on the drag coefficient (C_D) which is dependent on the particle shape and atmospheric condition. Transport and sedimentation of volcanic ash are complex processes, and the residence time and fall velocity of ash is critically dependent on particle size (Bonadonna et al., 1998), where with respect to the latter, smaller particles could be flowing in the atmosphere further from the vent.

Aerodynamic properties are important for safe aviation, and for studying the effects of volcanic ash on climate change, since these parameters determine the residence time of ash particles in the

71 atmosphere (e.g., Folch et al., 2009). The V_T of particles vary widely due to their irregular shapes and
72 material components (e.g., Wilson, 1972; Harris and Rose, 1983; Bonadonna et al., 2011, Maki et al.,
73 2016). Bonadonna et al. (2011) analyzed V_T of volcanic ash particle with various particle density (ρ_s)
74 from 990 to 2738 kg m⁻³ and Maki et al. (2016) summarized the list of various V_T relationships
75 suggested by previous studies. Volcanic ash particles have a range of shapes, and this presents a major
76 challenge when analyzing their characteristics. Recently, the irregularity of volcanic ash particles was
77 analyzed in detail based on the features of various regular particles, such as cubes, cylinders, and disks
78 (Bagheri and Bonadonna, 2016), using a computed tomography (CT) scanner (Dioguardi et al., 2017;
79 Garboczi and Bullard, 2017).

80 There are two approaches to studying these aerodynamic properties. The first approach is
81 theoretical, where a numerical simulation model is used to calculate terminal velocities, drag force,
82 and Reynolds number (Re); examples of this approach can be found in Happel and Brenner (2012).
83 The second approach is related to experimental research, in which the aforementioned relationships
84 are determined experimentally. For instance, Bagheri et al. (2013) and Bagheri and Bonadonna (2016)
85 analyzed the aerodynamic features of irregular shaped ash particle from the free fall experiments.
86 Dioguardi et al. (2018) suggested a new model of fluid drag for irregular shaped particles using various
87 previous researches. Since the aerodynamic feature depends on atmospheric condition and it can affect
88 the retrieval of V_T , it would be suggested that it can be analyzed through the free-fall laboratory
89 experiments for the following main reasons: 1) there is few chance to measure natural falling ash
90 particles. 2) it can be possible to control the size of ash particle in the free fall experiments. 3) and can
91 reduce wind effect in the experiments.

92 The present study applies the second approach (experimental research) to clarify the physical
93 characteristics of volcanic ash particles analyzing the experimental data. The rest of this paper is
94 organized as follows. Section 2 describes the free-fall experiments of ash particles and methods of

95 analysis. Section 3 presents the results of the free fall experiments. Section 4 is discussions and section

96 5 summarizes the results.

97

98 **2. Data and Methods**

99

100 **a. Two dimensional (2D) video disdrometer**

101 The 2D video disdrometer (2DVD) was developed by Joanneum Research (Graz, Austria) to detect
102 single raindrop particles, and the instrument has been modified to cover the errors caused by turbulence
103 effects (Nešpor et al., 2000). The device is able to observe the shape, V_T , and β of a single particle
104 using optical light. The ability to analyze a single particle is a significant advantage compared to other
105 disdrometers, such as the Joss-Waldvogel disdrometer (Joss and Waldvogel, 1967), the Precipitation
106 Occurrence Sensor System (Sheppard, 1990), and Parsivel (Löffler-Mang and Joss 2000). For instance,
107 Parsivel considers a fixed measurement area without any consideration of particle shape (e.g., Tokay
108 et al., 2014), while 2DVD observes particles by passing them through a 100 cm² observation area
109 consisting of two light sources and reflecting mirrors and two cameras, one set 6.2 mm above the other,
110 and collects data with a resolution of 630 pixels; this results in a pixel size of 0.2 mm at 55 kHz (Kruger
111 and Krajewski, 2002). Particles passing through the observation area yield shape information
112 according to the radiation intensity of the light sources, which is helpful for calculation of γ and β . The
113 V_T of particles is calculated using the height difference between the two cameras. Based on these
114 advantages, the oscillation and particle shape of raindrops can be analyzed by 2DVD (Thurai and
115 Bringi, 2005). Böhm (1989) analyzed the aerodynamic properties of an irregular hydrometeor and
116 Huang et al. (2010, 2015) used 2DVD to analyze the features of irregularly shaped snow. There have
117 been few previous aerodynamic analyses of volcanic ash particles performed using 2DVD, which is
118 able to detect and analyze volcanic ash particles with a range of irregular shapes. Thus, 2DVD offers
119 a unique approach as a new observation strategy.

120

121

122 **b. Definition of particle shape type**

123 Volcanic ash particles have various shapes that can be detected by 2DVD (Fig. 1). In the case of
124 raindrops, the DSD is dependent upon the break-up and coalescence processes occurring via up and
125 downdrafts, since the forces of gravity and buoyancy can easily affect raindrop shapes (Rosenfeld and
126 Ulbrich, 2003). However, solid particles do not readily change shape when falling without the
127 influence of forces such as collision. It is thus inferred that many particle shapes would be found in the
128 atmosphere, and that it would be possible to define and classify each particle shape type if we were
129 able to accurately detect a single particle. Thus, the range of γ for solid particles would be expected to
130 be wide compared to that of raindrops, and various values of V_T and β would likely be observed. The
131 γ_x of a particle is defined as the ratio of height to width for the observation direction x , and its
132 representative value is calculated using the geometric means of the two γ (γ_1, γ_2) detected by cameras
133 1 and 2, respectively (Eq. 1):

134

$$135 \gamma_{1(2)} = \frac{\text{Height}_{1(2)}}{\text{Width}_{1(2)}}, \quad \gamma = \sqrt{\gamma_1 \gamma_2}$$

136

137 Eq. (1).

138

139 The difference in angle between the rotating symmetric axis and vertical axis is defined as β . The
140 counter-clockwise (clockwise) movement of the rotating symmetric axis has a positive (negative) value
141 and the entire range is 180° (from -90° to 90°) with 0° as the center.

142 It is necessary to consider the true axis ratio (γ_T) to correctly define the particle shape (Fig. 2). The
143 apparent axis ratio (γ_A) considers the effect of β but the γ_T does not. The 2D coordinates (x, z) of the
144 particle shape with β are defined as follows:

145

146

$$x_A = r \cos(\theta + \beta), \quad z_A = r \sin(\theta + \beta)$$

147

148

$$x_T = r \cos\theta, \quad z_T = r \sin\theta$$

149

150

151

152

153

where subscript A is the coordinate of the original data coordinate considering the β and subscript T is the modified data coordinate. The symbol r refers to the length from the data point to the center and the symbol θ represents the degrees of data coordinates from the positive x axis, which range between 0° and 180° . In this paper, γ stands for γ_A for convenience.

154

155

156

157

158

159

160

161

162

163

An objective criterion for particle shape type was considered since particle shapes can be highly diverse and irregular (e.g., Bagheri and Bonadonna, 2016; Dioguardi et al., 2017; Garboczi and Bullard, 2017; Dioguardi et al., 2018). In the case of irregular particles, the γ can change according to the observation direction; however, any criterion should be able to define the particle shape types strictly and reliably. To solve this problem, particles with a rotating symmetric axis were the main target of the present study. Therefore, we considered oblate spheroid (O), prolate spheroid (P), and sphere (Sp), which all have a rotating symmetric axes. Among these particle types, the major axes of the oblate and prolate spheroids could be horizontally (H) and vertically (V) oriented with respect to the ground, respectively. Thus, the various particle shapes were divided into five types as follows; OH, OV, PH, PV, and Sp.

164

165

166

167

168

To define these particle shape types, a strict definition of the γ_T is required, which can be calculated from the β . As with the γ , the two β values are automatically calculated by 2DVD. In the case where the β is assumed as 0° , the rotating symmetric axis for OH and PV can be defined, since it is observed for any observation direction parallel to the ground. However, in the case of OV and PH particles, the rotating symmetric axis cannot be defined when the observation direction is parallel. In the case where

169 the β is not 0° , γ_T for all particle shape types would not change when oscillation occurs in a direction
170 orthogonal to the observation direction, but it is difficult to estimate both γ_T and β when particle
171 oscillation appears in a direction parallel to the observation direction. The ability to restore the γ_T and
172 β relative to this observation direction is limited, which is one of the main disadvantages of the 2D
173 observation strategy.

174 Based on these facts, a major β was selected based on the following reasoning: i) a β for the
175 observation direction with lower (higher) γ_T for OH (PV) is selected. ii) in the case of OV (PH), for
176 which the rotating symmetric axis was observed for only one observation direction, β was considered
177 where the value of β had a higher (lower) γ_T than that of the other observation direction. Therefore, β
178 with a lower (higher) γ_T in two observation directions for the case of an oblate (prolate) particle was
179 considered as a meaningful value. The perfect sphere could not have their value of β determined
180 theoretically, because there is the possibility of a rotating symmetric axis in any direction.

181 Based on the definition of β (Fig. 2), the perfect condition with respect to ellipsoids is satisfied
182 when $|\beta| = 0^\circ (90^\circ)$ for OH and PV (OV and PH); these values are defined as the center values. However,
183 2DVD calculated that the β for each particle shape type was concentrated around $|\beta| = 0^\circ (90^\circ)$ with
184 respect to horizontally (vertically) oriented particles, which correspond to OH and PH (OV and PV).
185 Furthermore, analysis of particles with an orthogonal center angle from 0° is difficult, since they have
186 two center angles ($\pm 90^\circ$). To address observation errors and enhance the convenience of analysis, all
187 center angles were set to $|\beta| = 0^\circ$ and modified to give the representative canting angle, β_R , using the
188 following equation:

189

190

$$\beta_R = \beta - \beta_0$$

191

192 where β_0 is the orienting angle, defined by the central angle of oscillation. In the case of vertically
193 oriented particles (OV and PV), β_0 could be defined as $\pm 90^\circ$. The sign of β_0 follows that of β .

194 After removing β , each particle shape was defined using γ_T (Table 1). Note that a 10% bias range
195 was allowed, to take observational error into account. For example, a particle was considered as a
196 sphere when $0.9 < \gamma_T < 1.1$, which is an applied 10% bias range from $\gamma_T = 1$. In addition, the particle
197 types OH and PV (OV and PH) were classified when the value of $|\gamma_1 - \gamma_2|$ was smaller (larger) than
198 $0.1\gamma_T$, to consider particles with only a rotating symmetric axis.

199

200

201 **c. Calculate the terminal velocity for the various particle shape types**

202 The V_T of volcanic ash is required to estimate the R_A ($\text{kg m}^{-2} \text{s}^{-1}$) on the ground where this depends
203 on atmospheric density (ρ_g in g cm^{-3}), T , Re , C_D , D , ρ_s , and its shape. Kunii and Levenspiel (1969)
204 developed a theoretical V_T equation:

205

$$206 \quad V_T = \left(\frac{4(\rho_s - \rho_g)gD}{3\rho_g C_D} \right)^{0.5} \quad (10^0 < Re < 10^4)$$

207 Eq. (2)

208

209 Later, Suzuki (1983) developed a theoretical V_T equation for tephra. Bonadonna et al. (2011) then
210 modified the theoretical V_T equation suggested by Kunii and Levenspiel (1969) with observed ash data,
211 which implied that the result of the theoretical V_T equation could be unsuitable for non-spherical
212 particles. Based on these equations, various C_D equations considering non-spherical particles were
213 subsequently developed. Tran-Cong et al. (2004) developed a new equation for C_D using the function

214 of circularity and Hölzer and Sommerfeld (2008) introduced a progressed C_D equation considering two
 215 types of sphericity: lengthwise ($\Phi_{||}$) and crosswise (Φ_{\perp}). This equation is as follows:

216

$$217 \quad C_D = \frac{8}{Re} \frac{1}{\sqrt{\Phi_{||}}} + \frac{16}{Re} \frac{1}{\sqrt{\Phi}} + \frac{3}{\sqrt{Re}} \frac{1}{\Phi^{3/4}} + 0.42 \times 10^{0.41(-\log(\Phi))^{0.2}} \frac{1}{\Phi_{\perp}}$$

218

Eq. (3)

219

220 The Re is defined as:

221

$$222 \quad Re = \frac{\rho_g V_T D}{\mu}$$

223

Eq. (4)

224

225 where μ is the dynamic viscosity ($\text{kg m}^{-1} \text{s}^{-1}$), which we assumed to be 1.983×10^{-5} based on
 226 atmospheric conditions at a T of $25 \text{ }^\circ\text{C}$. Three types of sphericity were defined as follows:

227

$$228 \quad \Phi = \frac{\pi D^2}{SA}$$

229

Eq. (5)

230

231 where SA is the surface area of the particle (mm^2). The lengthwise sphericity is defined as the ratio
 232 between the cross-sectional area of the volume-equivalent sphere and the difference between half the
 233 surface area and the mean of the projected vertical cross-sectional area (A_V) of the particle (Eq. 6):

234

$$235 \quad \Phi_{||} = \frac{\pi D^2}{4(0.5 \times SA - A_V)}$$

236

Eq. (6)

237

238

239

The crosswise sphericity is the same as the lengthwise sphericity, except for the denominator, which includes the projected horizontal cross-sectional area of the particle (A_H), defined as follows:

240

241

$$\Phi_{\perp} = \frac{\pi D^2}{4A_H}$$

242

Eq. (7)

243

244

It is noteworthy that the V_T is required to calculate the Re and V_T , which refers to the final product.

245

To solve this problem, the theoretical V_T (Eq. 2) was used as the input value of Eq. 4 until Eq. 2

246

converged.

247

248

249

d. Sakurajima volcano

250

Japan has around 10% (110) of all of the active volcanos in the world. Sakurajima (1,117m, 31.58°

251

N, 130.65° E, Kyushu, Japan) is an active volcanic island formed around 13,000 years ago, and its

252

tephra is approximately 60–66 % S_iO_2 Peléan-type (Oguchi et al., 2009; Takahashi et al., 2013). The

253

major eruptive events in historic age of Sakurajima were 1471–1476 (Bunmei era), 1779–1782 (An-ei

254

era) and 1914 (Taisho era). Sakurajima is an andesitic volcano with two peaks (Kita-dake and Minami-

255

dake). Volcanic activity at Kita-dake ended around 4,900 years ago then it changed to Minami-dake.

256

Activity has centred on Showa crater from 2006 (Iguchi, 2013). Showa crater is located on the eastern

257

flank approximately 500 m east of Minami-dake (Southern Peak) of Sakurajima volcano. It was

258

appeared in 1939 after one month of eruptions that year (Yokoo and Ishihara, 2007). The Minami-dake

259

summit crater was the only active center of Sakurajima volcano until the recommencement of Showa

260 crater from 1948 to 2006. The eruptive activity of Showa crater was resumed in June 2006 and
261 vulcanian eruptions gradually increased in the autumn of 2009 (Hotta et al., 2016). The Japan
262 Meteorological Agency (JMA) reported that the eruption frequency of Sakurajima would increase
263 significantly from 2009 and the accumulated ash fall exceeded 3.5 kg m^{-2} in Kagoshima city in 2012.
264 The Ministry of Land, Infrastructure, Transport, and Tourism (MLITT) installed an operational X-
265 band radar 10.7 km from the vent, as well as 16 automatic volcanic ash weight measurements, to
266 observe volcanic eruptions in 2011 (Fig. 3).

267

268

269 **e. Free fall experiments**

270 The data were collected by automatic volcanic ash weight measurements performed on the
271 Sakurajima volcano (Tajima et al., 2015; Maki et al., 2014; 2016). The free-fall experiments were
272 divided into two types; one was performed for each phi scale ($\Phi = -\log_2 D$) from $\Phi = 3$ to -4 ($0.125 <$
273 $D < 16 \text{ mm}$), and the other was not considered on a particle size scale. The former data, expressed by
274 A and B (Type 1), were collected at two sites and screened by size (Fig. 4); the latter data, expressed
275 as C–E (Type 2), were collected at 18 sites (Table 2). Free-fall experiments on collected volcanic ash
276 particles were carried out in the large-scale rainfall simulator of the National Research Institute for
277 Earth Science and Disaster Prevention (NIED) in Tsukuba, Japan. The collected particles were dropped
278 manually around 17 m from the ground and re-collected by a third-generation 2DVD (Maki et al.,
279 2016). Each sample was dropped for 30 sec to stimulate dispersion, and the measurement period was
280 1 min. To avoid wind effects including turbulence, the 2DVD was surrounded by a 3^3 cubic meter
281 windbreaking wall (Fig. 5).

282 The free-fall experiments were conducted at intervals of 1 min over 6 h 30 min, as shown in Fig.
283 6. The number of particles detected by 2DVD was less than 10,000 for 1 min, and the particle size

284 range of Type1 data set was proportional to its phi-scale, since small particles may be contained by
285 screening.

286 Figure 7 shows the distribution of raw data (the number of data: 274,215) for V_T and γ with D .
287 There were various γ from 0 to 2 when $D < 2$ mm and most of the data were concentrated near $\gamma = 0$.
288 The γ values converged around 1 and their distributional range decreased with D . The median value
289 with a 0.25 mm D interval corresponded well to the center of the data contour. The median line
290 converged around $\gamma = 0.935$ based on the correlation coefficient value (CC). When this was higher
291 than 0.95 for each D interval, the data converged. According to this condition, the range of $2 < D < 5$
292 mm was satisfied and the mean value was calculated using these data. The V_T had a wider range when
293 $D < 2$ mm but the median line corresponded well to the center of the data (Fig. 7b). The line
294 representing the largest amount of data is lower than the volcanic ash discussed by Bonadonna et al.
295 (2011). To select a available range of D , a theoretical terminal velocity equation ($V_{T,Ref}$) for a non-
296 sphere corresponding to Eqs. 2–7 was used as the reference. The particle density associated with the
297 eruption of Sakurajima volcano is between 2.43 and 2.59 g cm⁻³ (Oguchi et al., 2009), but the actual
298 particles contain air vacuoles (Van Eaton et al., 2012). This means that ρ_s , including vacuoles, is
299 smaller than ρ_s . Therefore, the minimum ρ_s was considered to be 2.43 g cm⁻³, and this was used as an
300 input parameter. The atmospheric conditions of T and P were considered from an automatic weather
301 station (AWS), supported by the JMA. The falling height of a particle which follows the
302 aforementioned conditions ($\gamma = 0.935$, $\rho_s = 2.43$ g cm⁻³) when $D = 4$ was lower than that under the
303 condition of free fall experiment (17 m) when it reached 90% of V_T (13.9 m); therefore, the available
304 data range is considered to be $D \leq 4$ mm, and this would satisfy the terminal fall velocity. The detailed
305 equations used in the present study are shown in Appendix A.

306

307

308 **f. Quality control procedures**

309 The 2DVD was originally developed to detect raindrop hydrometeors. For this reason, additional
310 quality control (QC) checks were deemed necessary to ensure applicability to non-hydrometeors, such
311 as volcanic ash particles. Specifically, we performed the following three QC procedures for accurate
312 analysis of the data:

313 i) Particle $D > 0.25$ mm was selected in consideration of the minimum spatial resolution of 2DVD.

314 ii) If the major axis observed by 2DVD was 10% longer than that of the value calculated directly
315 based on data coordinates, the data were considered erroneous and thus removed. A 10% bias range
316 was considered due to mathematical error, the irregular particle shape, and the limitation of the
317 spatiotemporal resolution of 2DVD.

318 iii) To consider volcanic ash particle, the sample satisfying in the certain range of terminal velocity
319 relationship was selected. If we consider a single V_T QC measure for the entire particle shape types, a
320 number of available data will be removed since V_T critically depends on particle shape. Therefore, we
321 applied a 60% V_T QC threshold (Jaffrain et al., 2011) for each particle shape type. It could be applied
322 once V_T relationship of volcanic ash particles is obtained. After selecting the particle shape types and
323 applying these two QC procedures (i and ii), 19.31% of the data (62,953) remained (Table 1).

324

325

326

327

328 **3. Results**

329

330 **a. Ash particle shape**

331 The ash particle size over the entire volcanic ash sample was skewed leftward, and the dominant
332 particle shape type changed with particle size (Fig. 8). The particles were predominantly horizontally
333 oriented (75.51%) and vertically oriented (21.60%). Oblate and prolate spheroids made up 76.26% and
334 23.85% of the particles, respectively. Hence, the particles were mainly OH (57.38%) or PH (15.88%)
335 (Table 2). The particles were predominantly $0.25 < D < 0.5$ mm (63.00%) or $0.5 < D < 1$ mm (32.80%).
336 Relatively few particles had $D > 1$ mm (4.20%).

337 There was large variation in shape among particles $0.25 < D < 0.5$ mm, but the variation decreased
338 with increasing D . All of the particle shape types had the largest number of particle at $D > 1.0$ mm and
339 the next were shown at $0.5 < D < 1.0$ mm, except for OH. In total, 95.80% of OH particles had $D < 1$
340 mm; at $D < 0.5$ mm, the value was 75.68%, and at $D = 0.5-1$ mm, it was 22.36%. In the cases of PH
341 and OV, 93.63% and 93.87% of these particles, respectively, had $D < 1$ mm. Beyond $D > 1$ mm, the
342 differences in the number of particles for each particle shape type were considerably decreased.

343

344

345 **b. Terminal velocity**

346 The V_T for the entire particle shape types well follows a polynomial regression analysis which was
347 applied to define the nonlinear relationship between V_T and D (Fig. 9a). It corresponds to that obtained
348 by Miwa et al (2015), who analyzed Parsivel data using the same laboratory experiments. There was
349 the inflection point of V_T at $D < 1.3$ mm and it came from an increase in the number of OH and an
350 decrease in their V_T when $D < 1$ mm. It can be seen the V_T relationship for each particle shape type.

351 The observed values of V_T were well classified by particle shapes (Fig. 9b). The highest values of
352 V_T were recorded in the order of prolate, sphere, and oblate. Vertically oriented particles had higher
353 V_T values than horizontal ones. The V_T for every particle type can be expressed in a power-law form,
354 except for OH. OH particles followed the regression line relatively closely, and showed the highest
355 CC and root mean square error (RMSE) values, of 0.94 and 0.46 m s^{-1} , respectively. Horizontally
356 orientated particles had relatively higher correlations (OH: 0.94, PH: 0.87) compared to those with a
357 vertical orientation (OV: 0.75, PV: 0.71). The V_T relationships and those of statistical parameters are
358 summarized in Table 3.

359 To verify the reliability of the particle data obtained by 2DVD, which was originally developed to
360 detect liquid raindrops, ρ_s , C_D , and Re , as well as theoretical V_T values according to these parameters,
361 were analyzed. To calculate the parameters of interest, including the surface area and cross-sectional
362 area of irregular particles, we applied the irregular particle volume estimation equations of Huang et
363 al. (2010).

364

365

366 **c. Aerodynamic properties**

367 Particle densities were estimated using the $V_{T,Ref}$, converged to 2.37 g cm^{-3} when $D < 1.5 \text{ mm}$ (Fig.
368 10a). This value corresponds well to that of the minimum ρ_s (2.43 g cm^{-3}) reported by Oguchi et al.
369 (2009). The slight difference is likely due to observation errors and the presence of vesicles (e.g.,
370 Seligman et al., 2016). The median value of ρ_s is changed to $0.5 < D < 1.5 \text{ mm}$, and this range
371 corresponds to that of V_T . Horizontally oriented particles (OH and PH) have relatively smaller ρ_s and
372 vertically oriented particles (OV and PV) have higher density (Fig. 10b); spheres have particle
373 densities that accord best with D . The median ρ_s values for all particle shapes converged when $D < 2$
374 mm, and the converged ρ_s values ranged from 2.35 to 2.50 g cm^{-3} .

375 The Re and C_D for the all particle shapes ranged from 10 to 4,000 and 0.6 to 20, respectively (Fig.
376 11a). Higher values of C_D were observed when $\log(Re) < 1.845$ ($Re < 70$); above this threshold, C_D
377 dramatically decreased. These results were derived according to the number of OH particles, which
378 mainly had $D < 0.5$ mm, and had higher C_D and lower Re . Particle shape was divided into two types:
379 OH and others (Fig. 11b). OH particles had higher C_D compared to the other particle shapes, which in
380 turn showed few differences among themselves. The OH particles experience strong drag forces under
381 the same flow conditions, leading to lower V_T . The differences between OH and other particles
382 diminished with $Re < 1,000$. The other particle shapes had relatively higher C_D in the range $10 < Re <$
383 $3,000$. Rong et al. (2015) analyzed the relationship between Re and C_D for oblate and prolate particles,
384 and showed that OH particles had higher C_D compared to the reference line (Clift and Gauven, 1971)
385 in the range $0 < Re < 400$. Each relationship is summarized in Fig. 11.

386

387

388 **d. Axis ratio**

389 The γ of a particle affects the backscattering power of electromagnetic waves, and it is necessary
390 to calculate the horizontal reflectivity (Z in dBZ), differential reflectivity (Z_{DR} in dB), and specific
391 differential phase shift (K_{DP} in $^{\circ} \text{ km}^{-1}$). Note that previous studies have analyzed the γ distribution for
392 raindrops and snow, including hail; however, few studies have been reported on γ of ash particles
393 compared to those for hydrometeor.

394 Figure 12 shows the quartiles and median values of γ for the entire particle shapes, and for each
395 individual particle shape type. The γ had a higher standard deviation (σ_{γ}) of > 0.25 when $D < 0.75$ mm,
396 which decreased and converged to $\sigma_{\gamma} = 0.15$ when $D > 1$ mm (Fig. 12a). The γ in the lower σ_{γ} range
397 converged to $\gamma = 0.94$ and could be expressed as follows:

398

399
$$\gamma(D) = 0.94 - 0.25\exp(-1.90 D)$$

400 Eq. (8)

401 The particles are more easily classified by shape than by V_T (Fig. 12b). Every particle shape type
402 was independent of D , except for OH. The γ of each particle types are expressed the following
403 relationships (Eqs. 9–12):

404
405
$$\gamma(D)_{OH} = 0.37 \tanh(1.84D - 1.88) + 0.38$$

406 Eq. (9)

407
$$\gamma_{OV} = 1.15$$

408 Eq. (10)

409
$$\gamma_{PH} = 0.88$$

410 Eq. (11)

411
$$\gamma_{PV} = 1.24$$

412 Eq. (12)

413

414 The parameter $\gamma(D)_{OH}$ was calculated using the hyperbolic tangent (\tanh) for the following reasons:
415 i) its range of values was wider than those of other particle types; ii) the data distribution changed
416 continuously with D ; and iii) it was present in a higher proportion (30.44%) compared to the other
417 parameters. We found that variations in γ decreased with D and the proportion of Sp shapes increased
418 when $D > 2$ mm. The particle types OV and PH showed a wide distribution over $1 < \gamma < 1.5$ and $0.4 <$
419 $\gamma < 1.0$, respectively, when $D < 2$ mm, but the variability in median values was relatively low. The
420 relationships of γ for each particle shape type could be expressed by constant values at $\gamma = 0.75$ (OH),
421 0.88 (PH), 1.15 (OV), and 1.24 (PV), respectively, and these differences are around $\gamma = 0.12$.

422

423

424 **e. Canting angle**

425 Statistical analysis of β is required to understand the aerodynamic properties of volcanic ash
426 particles, and the input parameters of T-matrix scattering simulations, to verify the observed radar
427 variables. The histogram of β_R can be shown in Fig. 13

428 More than 95% of β values for each particle shape type were concentrated in the range $|\beta_R| \leq 30^\circ$,
429 with 0° as the center (Fig. 13). The particles were symmetrically distributed around 0° and more than
430 50% were concentrated in the range $|\beta_R| < 4^\circ$. The horizontally oriented β distribution was relatively
431 narrow ($|\beta_R| < 20^\circ$) and exhibited a unimodal distribution. It is noteworthy that 90% of OH particles
432 were concentrated in the range $|\beta_R| < 4^\circ$. The vertically oriented β distribution was relatively broader
433 ($|\beta_R| < 30^\circ$) and followed a bimodal distribution. PV exhibited a bimodal form, but this was not
434 symmetrical about 0° . For spheres, the β distribution was narrower, similar to horizontally oriented
435 particles, and it had a bimodal distribution, similar to vertically oriented particles, indicating that the
436 independent features of both orientations were combined.

437 The values of $|\overline{\beta_R}|$ and $|\sigma_\beta|$ for OH and PV (OV, PH) were 0° and 3.5° (0.4° , 13.1°), and 1.3° and
438 12.7° (0.2° , 10.9°), respectively. OV (OH) had the highest (lowest) value of $|\sigma_\beta|$. This validates the
439 assumption of Marzano et al. (2012) under stable conditions ($|\sigma_\beta| = 10^\circ$). Therefore, we believe that
440 the tumbling phenomenon ($|\sigma_\beta| > 30^\circ$) of the particles under calm atmospheric conditions was likely to
441 be minor.

442 To analyze the correlation between particle D and β , quartiles for each particle D interval were
443 calculated (Fig. 14). The particles were concentrated at $|\beta_R| < 30^\circ$ regardless of D, and median values
444 were stable when $D < 1$ mm for the entire particle shape types; however, fluctuation increased with D
445 (Fig. 14a). The $|\sigma_\beta|$ values gradually increased from 10° to 13° when $0.3 < D < 1.3$ mm and variability
446 was greatest around the center (13°). This increase in $|\sigma_\beta|$ would not be expected in the case of a

447 relatively small number of particles (Fig. 8a), since their standard deviation is largely maintained at
448 about 13° regardless of dataset size.

449 Variability in the median values for individual particles was more apparent. The values converged
450 around 0° but fluctuation increased with greater D from the zero line. The median $|\beta_R|$ values
451 exceeded 3° , 5° , 10° , and 15° when $D > 1$ mm, $1 < D < 2$ mm, $2 < D < 3$ mm, and $D > 3$ mm,
452 respectively (Fig. 14b).

453

4. Discussions

454

455 The results of present study can be extended in viewpoint of the radar meteorology: i) the radar
456 observation and ii) ashfall rate (R_A) estimations. i) Weather radar operates for a similar purpose to that
457 of meteorological satellites, and provides information for determining the volume, mass, and echo top
458 height of weather systems. Short-duration eruptions, i.e., less than 1 hour, can be detected at high
459 spatio-temporal resolution, especially in the early period of an eruption. The temporal resolution of
460 weather radar is a few minutes for a single volume scan, and depends on the observation strategy and
461 radar band. The spatial resolution of weather radar is a few hundred meters and is proportional to the
462 radar frequency. A number of ash cloud detections were reported in several observational cases in the
463 US and Japan (Maki and Doviak, 2001; Maki et al., 2012). Marzano et al. (2013) summarized 28 major
464 explosive volcanic eruptions detected by weather radars from 1970 to 2011. Harris and Rose (1983)
465 attempted to analyze volcanic ash particle size and total mass using a C-band weather radar. Maki and
466 Doviak (2001) proposed the method to retrieve PSD from radar measurements of volcanic ash and
467 Donnadieu et al. (2012) detected volcanic eruptions using an L-band fixed radar. Marzano et al. (2006,
468 2012) and Maki et al. (2012, 2014) detected and analyzed volcanic eruptions using weather radars,
469 from theoretical (physical) and experimental (engineering) perspectives. Thus, observability of
470 volcanic ash clouds using weather radar can be confirmed from previous researches. To verify radar-
471 based volcanic ash cloud observations, a scattering simulation can be considered. The basic parameters:
472 axis ratio, canting angle which are the results presented in this study are the input information of
473 scattering simulation to simulate the theoretical radar variables. In particular, the T-matrix scattering
474 simulation developed by Waterman (1965) is useful for calculation of the theoretical backscattering
475 power of non-spherical particles.

476 Seconds, the V_T is one of the main parameters for R_A ($\text{kg m}^{-2} \text{hr}^{-1}$) and it is defined in terms of PSD
477 and V_T as follows:

478

479

$$R_A = V_r \frac{3.6}{10^3} \int_{D_1}^{D_2} V_T(D) N(D) D^3 dD$$

480

Eq. (13)

481

482

where V_r is the particle volume ratio. In case of sphere, it is considered as $\pi/6$.

483

484

485

486

487

488

489

490

Marzano et al. (2012b) proposed Z- C_A relationships using the ashfall concentration (C_A in g m^{-3}) and z. Maki et al. (2016) introduced R_A -z relationship for Sakurajima eruption case (18. Aug. 2013) using the time integration of R_A (S_A in kg m^{-2}) obtained by automatic volcanic ash weight measurements. However, once we use the disdrometer such as 2DVD, it will be possible to estimate R_A directly since 2DVD can measure PSD, V_T and γ . Therefore, basic parameters could help to simulate radar variables and estimate R_A which are necessary to develop the quantitative ash fall estimation (QAE) method.

491 **5. Summary and Conclusions**

492 The basic parameters (V_T , γ and β) of volcanic ash particles were analyzed from the free fall
493 experiments with 2DVD. Data were collected with 18 automatic volcanic ash weight measurements
494 performed on Sakurajima volcano, Japan (31.58° N, 130.65° E). To identify the aerodynamic properties
495 of the volcanic ash particles in the samples, a free-fall experiment was conducted in the large-scale
496 rainfall simulator of the NIED, and 274,215 samples were analyzed.

497 Radar variables are highly dependent on the $|K|^2$, size, and shape of particles. Particle types with
498 rotating symmetric axes were assumed to represent volcanic ash particles which have a wide variety
499 of irregular shape. Their orientation was also considered with respect to horizontally (OH, PH) and
500 vertically (OV, PV) oriented oblate and prolate spheroids were studied, respectively.

501 The dominant particle shape comprised horizontally and vertical oriented particles, present in
502 proportions of 75.51% and 21.60%, respectively. Regarding particle shape, oblate (prolate) spheroids
503 comprised 76.26% (23.85%) of all particles in the samples. The most common particle shape type was
504 OH, accounting for 59% of all particles when $D < 1$ mm, and 69% when $D < 0.5$ mm. Overall, 95.80%,
505 93.87%, and 93.63% of the OH, OV, and PH particles had $D < 1$ mm, respectively.

506 The V_T of the particles were classified in the order of PV, OV, Sp, PH and OH. These results are
507 consistent with the $V_{T, Ref}$, which suggests that 2DVD is a reliable for observing volcanic ash particles
508 under stable weather conditions. A noticeable increase in V_T for OH in the range $0.5 < D < 1$ mm
509 occurred through an increase in γ ; this was not observed for other particle types.

510 The estimated ρ_s converged to 2.37g cm^{-3} when $D > 1.5$ mm, and the median value changed over
511 the range $0.5 < D < 1.5$ mm. The converged value of ρ_s is consistent with the value for the Sakurajima
512 volcano reported by Oguchi et al. (2009). The relationship of C_D and Re were divided into two particle
513 type categories (OH and the others) and $C_D(\text{OH})$ was dramatically increased in the range of $Re < 70$.
514 These results were derived from the particle concentration of OH, which was highest when $D < 0.5$

515 mm; at this threshold, C_D was higher and Re was lower. The range of V_T over $0.7 < D < 1.3$ mm was
516 informed by both γ and ρ_s .

517 The σ_γ decreased in the range of $D > 0.75$ mm, to 0.15, and converged to $\gamma = 0.94$. Maki et al.
518 (2014) introduced the radar variables and found that Z_{DR} gradually increased with time; the dominant
519 values at 10 and 18 min after the eruption were close to 1 and 2 dB, respectively. The results presented
520 in this study corresponded to volcanic eruption clouds with positive Z_{DR} since it is a function of $|K|^2$
521 and γ (Herzegg and Jameson, 1992). In addition, it can be explained that the size sorting of ash particle
522 (e.g., Beckett et al., 2015; Stevenson et al., 2015) will affect the increase of ZDR by the results of
523 present study.

524 The $|\sigma_\beta|$ of OV particles with $|\beta_0| = 90^\circ$ was largest (13.1°) among all particle types and OH particles
525 had the lowest $|\sigma_\beta|$ at 3.5° . Based on the $|\sigma_\beta|$ results, the tumbling phenomenon would not be dominant
526 under calm atmospheric conditions. The quartiles were stable when $D < 1$ mm for the entire particle
527 shape types, but increased with D . The value of σ_β was higher when $D < 1.3$ mm and started to converge
528 around 13° due to a decrease in the number of OH particles.

529 These results could be the essential information to develop the new approaches for detecting non-
530 hydrometeors and numerical model. The axis ratio and canting angle of ash particles obtained from
531 the present study are necessary for scattering simulations. V_T obtained by the present study suggests
532 that smaller particles can be transported longer distance. Therefore, it will be useful for scattering
533 simulation of ash particles to develop QAE and help to improve a numerical model using V_T obtained
534 by the present study.

535

536

Author contributions

537

Masato Iguchi and Masayuki Maki designed the study. Akihiko Yamaji and Tatsuya Momotani

538

collected the samples and performed the free-fall experiment. Sung-Ho Suh modified the original study

539

theme and performed the study. Masayuki Maki and Sung-Ho Suh performed research, obtained the

540

results and prepared the manuscript along with contributions from all of the co-authors. Dong-In Lee

541

examined the results and checked the manuscript.

542

543

Acknowledgments

544

This work was supported by a Grant-in Aid for JSPS KAKENHI (grant number JP16H03145) and

545

partially supported by a DPRI collaborative research grant (Kyoto Univ. 25G-11). The authors

546

acknowledge the provision of ashfall data and funding for this work from Kyoto and Kagoshima

547

Universities. The 2DVD data were provided by MEXT, Japan. We also thank the NIED for use of

548

their large-rainfall simulator.

549

550 **Appendix A**

551

552 The theoretical fall velocity and falling distance with time are calculated as follows;

553

554

$$F = ma = F_g - F_D$$

555

Eq. (A1)

556

$$F_g = mg$$

557

Eq. (A2)

558

$$F_D = \frac{1}{2} \rho_g V^2 C_D A$$

559

Eq. (A3)

560

561 where F_g is universal gravitation, F_D is drag force, m is mass, and a is the free-fall acceleration.

562 In Eq. A2, g is the acceleration due to gravity, considered to be 9.81 m s^{-2} , and V and C_D in Eq. A3

563 correspond to the values in Eq. 2–7. The symbols μ and ρ_g are the dynamic viscosity and density of

564 the atmosphere and were assumed as $1.837 \times 10^{-5} \text{ kg m}^{-1} \text{ s}^{-1}$ and $1.194 \times 10^{-5} \text{ g cm}^{-3}$, respectively.

565 The results were based on conditions at an atmospheric T as $25 \text{ }^\circ\text{C}$.

566 To ensure accuracy, we considered the surface roughness effect of a volcanic ash particle (1.07^{-1})

567 on the fall velocity, as suggested by Bagheri and Bonadonna (2016), and the results for $D = 4 \text{ mm}$

568 are shown in Fig. A1.

569 **References**

- 570 Böhm, H. P.: A general equation for the terminal fall speed of solid hydrometeors, *Journal of the*
571 *Atmospheric Sciences*, 46, 2419-2427, 1989.
- 572 Bagheri, G., Bonadonna, C., Manzella, I., Pontelandolfo, P., and Haas, P.: Dedicated vertical wind
573 tunnel for the study of sedimentation of non-spherical particles, *Review of Scientific*
574 *Instruments*, 84, 054501, 2013.
- 575 Bagheri, G. and Bonadonna, C.: On the drag of freely falling non-spherical particles, *Powder*
576 *Technology*, 301, 526-544, 2016.
- 577 Beckett, F., Witham, C., Hort, M., Stevenson, J., Bonadonna, C., and Millington, S.: Sensitivity of
578 dispersion model forecasts of volcanic ash clouds to the physical characteristics of the
579 particles, *Journal of Geophysical Research: Atmospheres*, 120, 2015.
- 580 Bonadonna, C., Ernst, G., and Sparks, R.: Thickness variations and volume estimates of tephra fall
581 deposits: the importance of particle Reynolds number, *Journal of Volcanology and*
582 *Geothermal Research*, 81, 173-187, 1998.
- 583 Bonadonna, C., Genco, R., Gouhier, M., Pistolesi, M., Cioni, R., Alfano, F., Hoskuldsson, A., and
584 Ripepe, M.: Tephra sedimentation during the 2010 Eyjafjallajökull eruption (Iceland)
585 from deposit, radar, and satellite observations, *Journal of Geophysical Research: Solid*
586 *Earth (1978–2012)*, 116, 2011.
- 587 Bonadonna, C., Folch, A., Loughlin, S., and Puempel, H.: Future developments in modelling and
588 monitoring of volcanic ash clouds: outcomes from the first IAVCEI-WMO workshop on
589 Ash Dispersal Forecast and Civil Aviation, *Bulletin of volcanology*, 74, 1-10, 2012.

590 Clift, R. and Gauvin, W.: Motion of particles in turbulent gas streams, *British Chemical Engineering*,
591 16, 229-236, 1971.

592 Coltelli, M., Miraglia, L., and Scollo, S.: Characterization of shape and terminal velocity of tephra
593 particles erupted during the 2002 eruption of Etna volcano, Italy, *Bulletin of volcanology*,
594 70, 1103-1112, 2008.

595 Del Bello, E., Taddeucci, J., Vitturi, M. d. M., Scarlato, P., Andronico, D., Scollo, S., Kueppers, U.,
596 and Ricci, T.: Effect of particle volume fraction on the settling velocity of volcanic ash
597 particles: insights from joint experimental and numerical simulations, *Scientific reports*,
598 7, 39620, 2017.

599 Dellino, P., Mele, D., Bonasia, R., Braia, G., La Volpe, L., and Sulpizio, R.: The analysis of the
600 influence of pumice shape on its terminal velocity, *Geophysical Research Letters*, 32,
601 2005.

602 Dioguardi, F., Mele, D., Dellino, P., and Dürig, T.: The terminal velocity of volcanic particles with
603 shape obtained from 3D X-ray microtomography, *Journal of Volcanology and Geothermal*
604 *Research*, 329, 41-53, 2017.

605 Dioguardi, F., Mele, D., and Dellino, P.: A New One-Equation Model of Fluid Drag for Irregularly
606 Shaped Particles Valid Over a Wide Range of Reynolds Number, *Journal of Geophysical*
607 *Research: Solid Earth*, 123, 144-156, 2018.

608 Donnadieu, F.: *Volcanological applications of Doppler radars: A review and examples from a*
609 *transportable pulse radar in L-band*, INTECH Open Access Publisher, 2012.

610 Folch, A., Costa, A., and Macedonio, G.: FALL3D: A computational model for transport and
611 deposition of volcanic ash, *Computers & Geosciences*, 35, 1334-1342, 2009.

612 Ganser, G. H.: A rational approach to drag prediction of spherical and nonspherical particles, Powder
613 Technology, 77, 143-152, 1993.

614 Garboczi, E. and Bullard, J.: 3D analytical mathematical models of random star-shape particles via a
615 combination of X-ray computed microtomography and spherical harmonic analysis,
616 Advanced Powder Technology, 28, 325-339, 2017.

617 Hölzer, A. and Sommerfeld, M.: New simple correlation formula for the drag coefficient of non-
618 spherical particles, Powder Technology, 184, 361-365, 2008.

619 Haider, A. and Levenspiel, O.: Drag coefficient and terminal velocity of spherical and nonspherical
620 particles, Powder technology, 58, 63-70, 1989.

621 Happel, J. and Brenner, H.: Low Reynolds number hydrodynamics: with special applications to
622 particulate media, Springer Science & Business Media, 2012.

623 Harris, D. M. and Rose, W. I.: Estimating particle sizes, concentrations, and total mass of ash in
624 volcanic clouds using weather radar, Journal of Geophysical Research: Oceans (1978–
625 2012), 88, 10969-10983, 1983.

626 Herzegh, P. H. and Jameson, A. R.: Observing precipitation through dual-polarization radar
627 measurements, Bulletin of the American Meteorological Society, 73, 1365-1376, 1992.

628 Hotta, K., Iguchi, M., and Tameguri, T.: Rapid dike intrusion into Sakurajima volcano on August 15,
629 2015, as detected by multi-parameter ground deformation observations, Earth, Planets and
630 Space, 68, 68, 2016.

631 Huang, G.-J., Bringi, V., Cifelli, R., Hudak, D., and Petersen, W.: A methodology to derive radar
632 reflectivity-liquid equivalent snow rate relations using C-band radar and a 2D video
633 disdrometer, Journal of Atmospheric and Oceanic Technology, 27, 637-651, 2010.

- 634 Huang, G.-J., Bringi, V., Moisseev, D., Petersen, W. A., Bliven, L., and Hudak, D.: Use of 2D-video
635 disdrometer to derive mean density–size and Z e–SR relations: Four snow cases from the
636 light precipitation validation experiment, *Atmospheric Research*, 153, 34-48, 2015.
- 637 Iguchi, M.: Magma Movement from the Deep to Shallow Sakurajima Volcano as Revealed by
638 Geophysical Observations (< Special Section> Sakurajima Special Issue), *Bulletin of the*
639 *Volcanological Society of Japan*, 58, 1-18, 2013.
- 640 Jaffrain, J., Studzinski, A., and Berne, A.: A network of disdrometers to quantify the small-scale
641 variability of the raindrop size distribution, *Water Resources Research*, 47, 2011.
- 642 Joss, J., and Waldvogel A.: A spectrograph for the automatic analysis of raindrops, *Pure and Applied*
643 *Geophysics*, 69, 240-246, 1967.
- 644 Kruger, A. and Krajewski, W. F.: Two-dimensional video disdrometer: A description, *Journal of*
645 *Atmospheric and Oceanic Technology*, 19, 602-617, 2002.
- 646 Kunii, D.: 0. Levenspiel, *Fluidization Engineering*, John Wiley, 8, 44-45, 1969.
- 647 Langmann, B., Folch, A., Hensch, M., and Matthias, V.: Volcanic ash over Europe during the eruption
648 of Eyjafjallajökull on Iceland, April–May 2010, *Atmospheric Environment*, 48, 1-8, 2012.
- 649 Löffler-Mang, M. and Joss, J.: An optical disdrometer for measuring size and velocity of hydrometeors,
650 *Journal of Atmospheric and Oceanic Technology*, 17, 130-139, 2000.
- 651 Maki, M. and Doviak, R.: Volcanic ash size distribution determined by weather radar, 1810-1811,
652 2001.
- 653 Maki, M., Maesaka, T., Kozono, T., Nagai, M., Furukawa, R., Nakada, S., Koshida, T., and Takenaka,
654 H.: Quantitative volcanic ash estimation by operational polarimetric weather radar, 2012.

- 655 Maki, M., Maesaka, T., Muraji, Y., and Suzuki, I.: Statistical analysis of volcanic ash measured by X-
656 band polarimetric radar, 2014.
- 657 Maki, M., Iguchi, M., Maesaka, T., Miwa, T., Tanada, T., Kozono, T., Momotani, T., Yamaji, A., and
658 Kakimoto, I.: Preliminary results of weather radar observations of sakurajima volcanic
659 smoke, *Journal of Disaster Research*, 11, 15-30, 2016.
- 660 Marzano, F. S., Barbieri, S., Vulpiani, G., and Rose, W. I.: Volcanic ash cloud retrieval by ground-
661 based microwave weather radar, *IEEE transactions on geoscience and remote sensing*, 44,
662 3235-3246, 2006.
- 663 Marzano, F. S., Picciotti, E., Vulpiani, G., and Montopoli, M.: Synthetic signatures of volcanic ash
664 cloud particles from X-band dual-polarization radar, *IEEE Transactions on Geoscience
665 and Remote Sensing*, 50, 193-211, 2012.
- 666 Marzano, F. S., Picciotti, E., Montopoli, M., and Vulpiani, G.: Inside volcanic clouds: Remote sensing
667 of ash plumes using microwave weather radars, *Bulletin of the American Meteorological
668 Society*, 94, 1567-1586, 2013.
- 669 Nešpor, V., Krajewski, W. F., and Kruger, A.: Wind-induced error of raindrop size distribution
670 measurement using a two-dimensional video disdrometer, *Journal of Atmospheric and
671 Oceanic Technology*, 17, 1483-1492, 2000.
- 672 Oguchi, T., Udagawa, M., Nanba, N., Maki, M., and Ishimine, Y.: Measurements of dielectric constant
673 of volcanic ash erupted from five volcanoes in Japan, *IEEE Transactions on Geoscience
674 and Remote Sensing*, 47, 1089-1096, 2009.

- 675 Poulidis, A. P., Takemi, T., Iguchi, M., and Renfrew, I. A.: Orographic effects on the transport and
676 deposition of volcanic ash: A case study of Mount Sakurajima, Japan, *Journal of*
677 *Geophysical Research: Atmospheres*, 122, 9332-9350, 2017.
- 678 Rong, L., Zhou, Z., and Yu, A.: Lattice–Boltzmann simulation of fluid flow through packed beds of
679 uniform ellipsoids, *Powder Technology*, 285, 146-156, 2015.
- 680 Rosenfeld, D. and Ulbrich, C. W.: Cloud microphysical properties, processes, and rainfall estimation
681 opportunities. In: *Radar and Atmospheric Science: A Collection of Essays in Honor of*
682 *David Atlas*, Springer, 2003.
- 683 Seligman, A. N., Bindeman, I. N., Watkins, J. M., and Ross, A. M.: Water in volcanic glass: From
684 volcanic degassing to secondary hydration, *Geochimica et Cosmochimica Acta*, 191, 216-
685 238, 2016.
- 686 Sheppard, B. E.: Measurement of raindrop size distributions using a small Doppler radar, *Journal of*
687 *Atmospheric and Oceanic Technology*, 7, 255-268, 1990.
- 688 Sigurdsson, H., Houghton, B., McNutt, S., Rymer, H., and Stix, J.: *The encyclopedia of volcanoes*,
689 Elsevier, 2015.
- 690 Stevenson, J., Millington, S., Beckett, F., Swindles, G., and Thordarson, T.: Big grains go far:
691 understanding the discrepancy between tephrochronology and satellite infrared
692 measurements of volcanic ash, *Atmospheric Measurement Techniques*, 8, 2069-2091,
693 2015.
- 694 Stokes, G. G.: *On the effect of the internal friction of fluids on the motion of pendulums*, Pitt Press
695 Cambridge, 1851.

696 Suzuki, T.: A theoretical model for dispersion of tephra, *Arc volcanism: physics and tectonics*, 95, 113,
697 1983.

698 Takahashi, M., Otsuka, T., Sako, H., Kawamata, H., Yasui, M., Kanamaru, T., Otsuki, M., Kobayashi,
699 T., Ishihara, K., and Miki, D.: Temporal Variation for Magmatic Chemistry of the
700 Sakurajima Volcano and Aira Caldera Region, Southern Kyushu, Southwest Japan since
701 61 ka and Its Implications for the Evolution of Magma Chamber System, *Bulletin of the*
702 *Volcanological Society of Japan*, 58, 19-42, 2013.

703 Tajima, Y., Ohara, D., Fukuda, K., and Shimomura, S.: Development of Automatic Tephrometer for
704 Monitoring of Volcano, 39-46, 2015.

705 Thurai, M. and Bringi, V.: Drop axis ratios from a 2D video disdrometer, *Journal of Atmospheric and*
706 *Oceanic Technology*, 22, 966-978, 2005.

707 Tokay, A., Wolff, D. B., and Petersen, W. A.: Evaluation of the new version of the laser-optical
708 disdrometer, OTT Parsivel2, *Journal of Atmospheric and Oceanic Technology*, 31, 1276-
709 1288, 2014.

710 Tran-Cong, S., Gay, M., and Michaelides, E. E.: Drag coefficients of irregularly shaped particles,
711 *Powder Technology*, 139, 21-32, 2004.

712 Van Eaton, A. R., Muirhead, J. D., Wilson, C. J., and Cimarelli, C.: Growth of volcanic ash aggregates
713 in the presence of liquid water and ice: an experimental approach, *Bulletin of volcanology*,
714 74, 1963-1984, 2012.

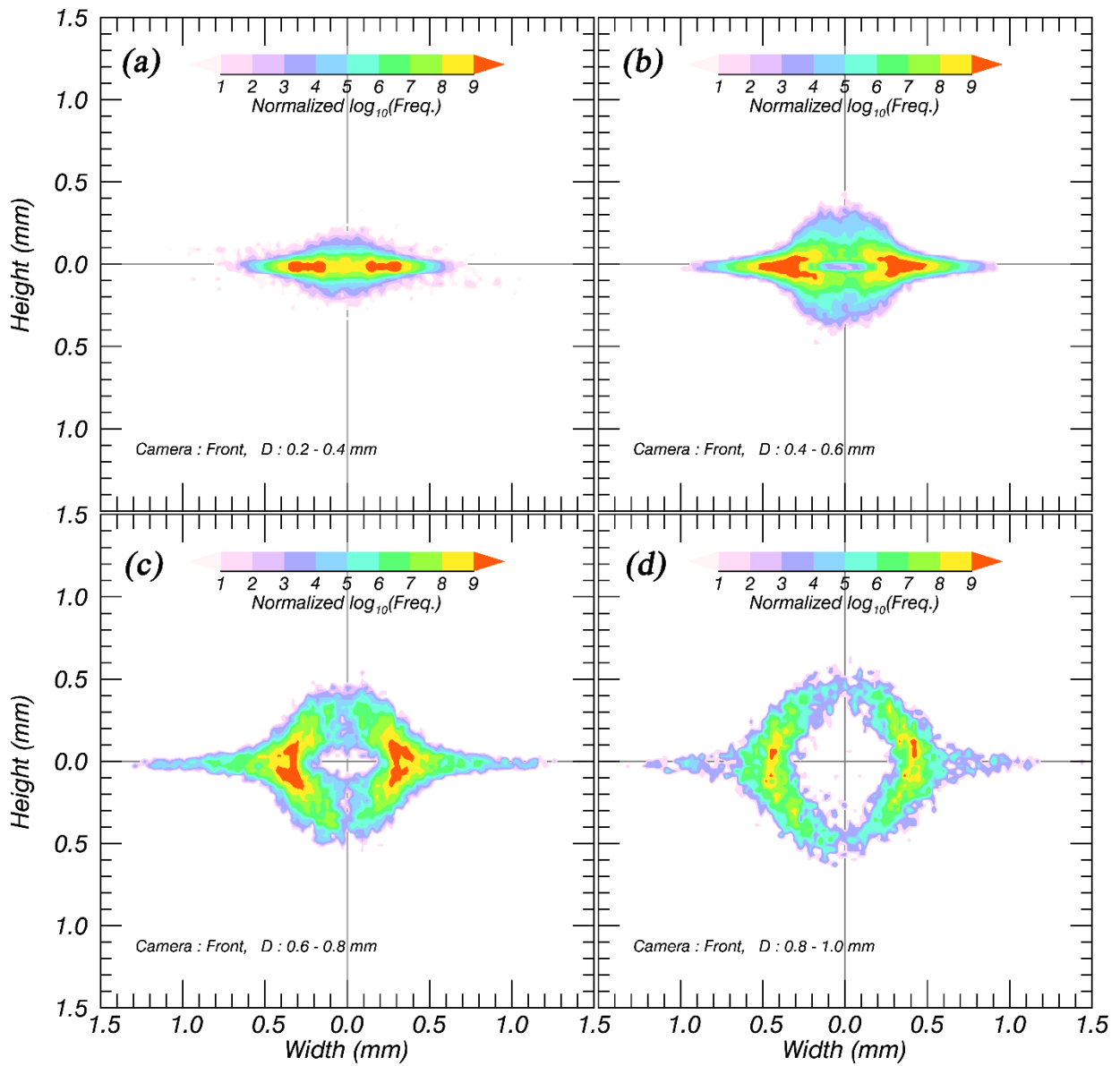
715 Waterman, P. C.: Symmetry, unitarity, and geometry in electromagnetic scattering, *Physical review D*,
716 3, 825, 1971.

- 717 Wilson, L. and Huang, T.: The influence of shape on the atmospheric settling velocity of volcanic ash
718 particles, *Earth and Planetary Science Letters*, 44, 311-324, 1979.
- 719 Wilson, T. M., Stewart, C., Sword-Daniels, V., Leonard, G. S., Johnston, D. M., Cole, J. W., Wardman,
720 J., Wilson, G., and Barnard, S. T.: Volcanic ash impacts on critical infrastructure, *Physics
721 and Chemistry of the Earth, Parts A/B/C*, 45, 5-23, 2012.
- 722 Wilson, T. M., Jenkins, S., and Stewart, C.: Impacts from volcanic ash fall. In: *Volcanic Hazards,
723 Risks and Disasters*, Elsevier, 2015.
- 724 Yokoo, A. and Ishihara, K.: Volcanic activity around Showa Crater of Sakurajima Volcano monitored
725 with infrared and video cameras, *Annals of Disas. Prev. Res. Inst., Kyoto Univ.*, No. 50
726 C., 2007.
- 727
- 728

729

Figures

730



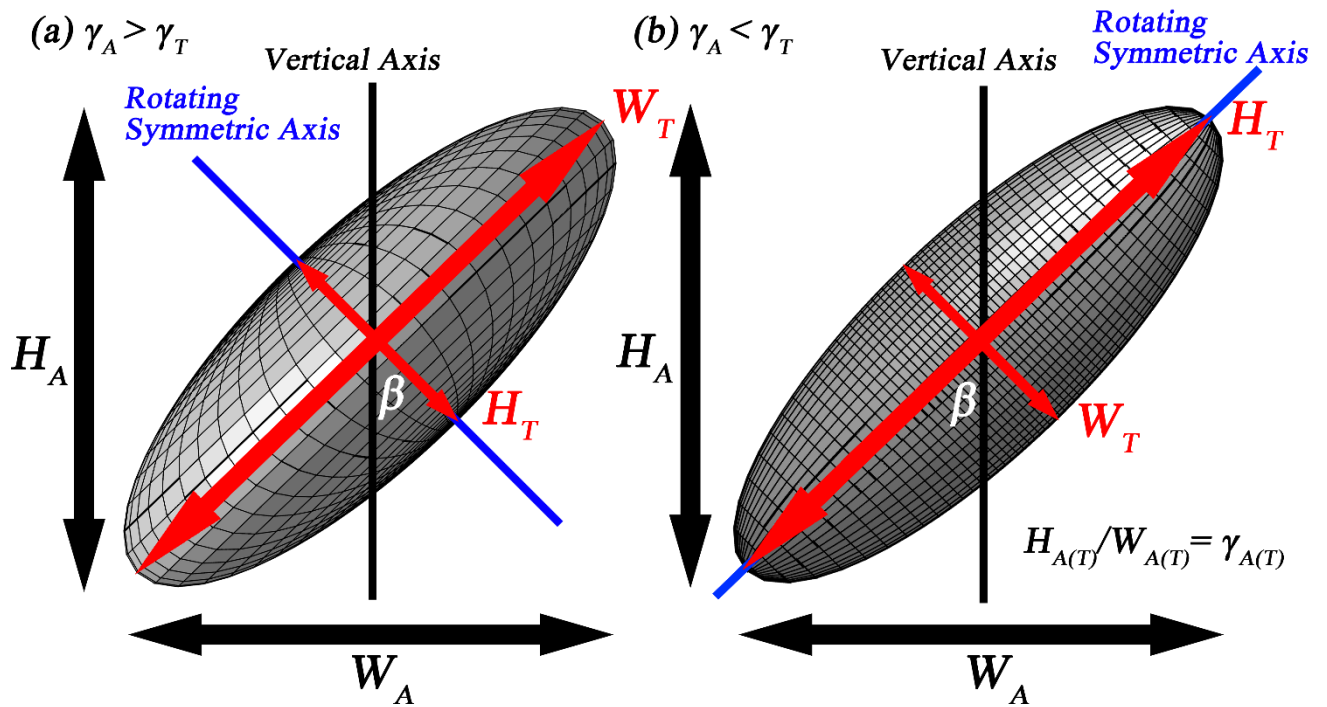
731

732 Figure 1. Accumulated contoured images of volcanic ash particles with D measured by a two-
733 dimensional video disdrometer (2DVD).

734

735

736



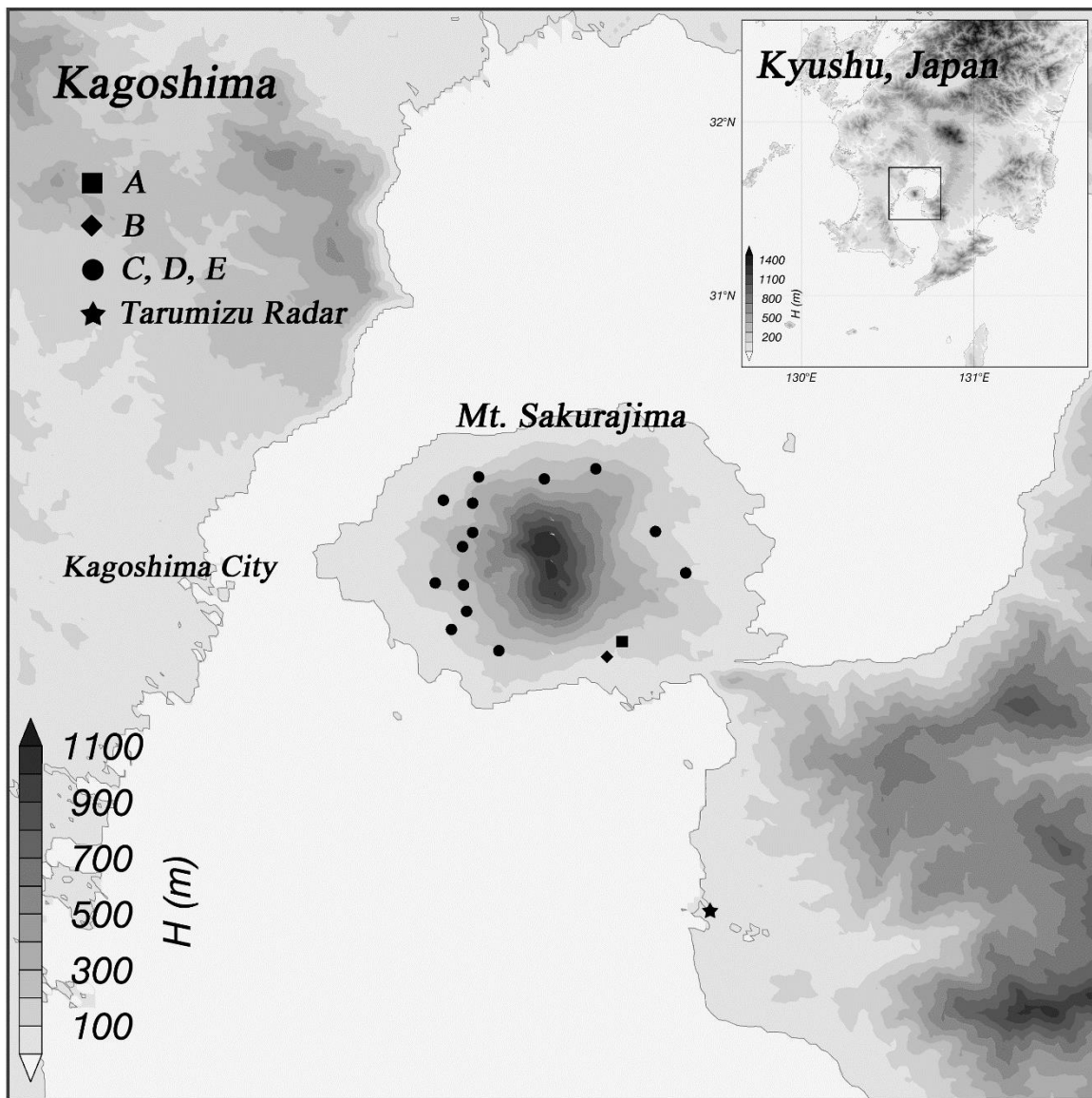
737

738 Figure 2. Conceptual model of an (a) oblate and (b) prolate spheroid with the same canting angle
 739 (β). $W_{A(T)}$ and $H_{A(T)}$ are the apparent (true) width and height of the particle, respectively. $\gamma_{A(T)}$ is the
 740 apparent (true) axis ratio.

741

742

743



744

745

746

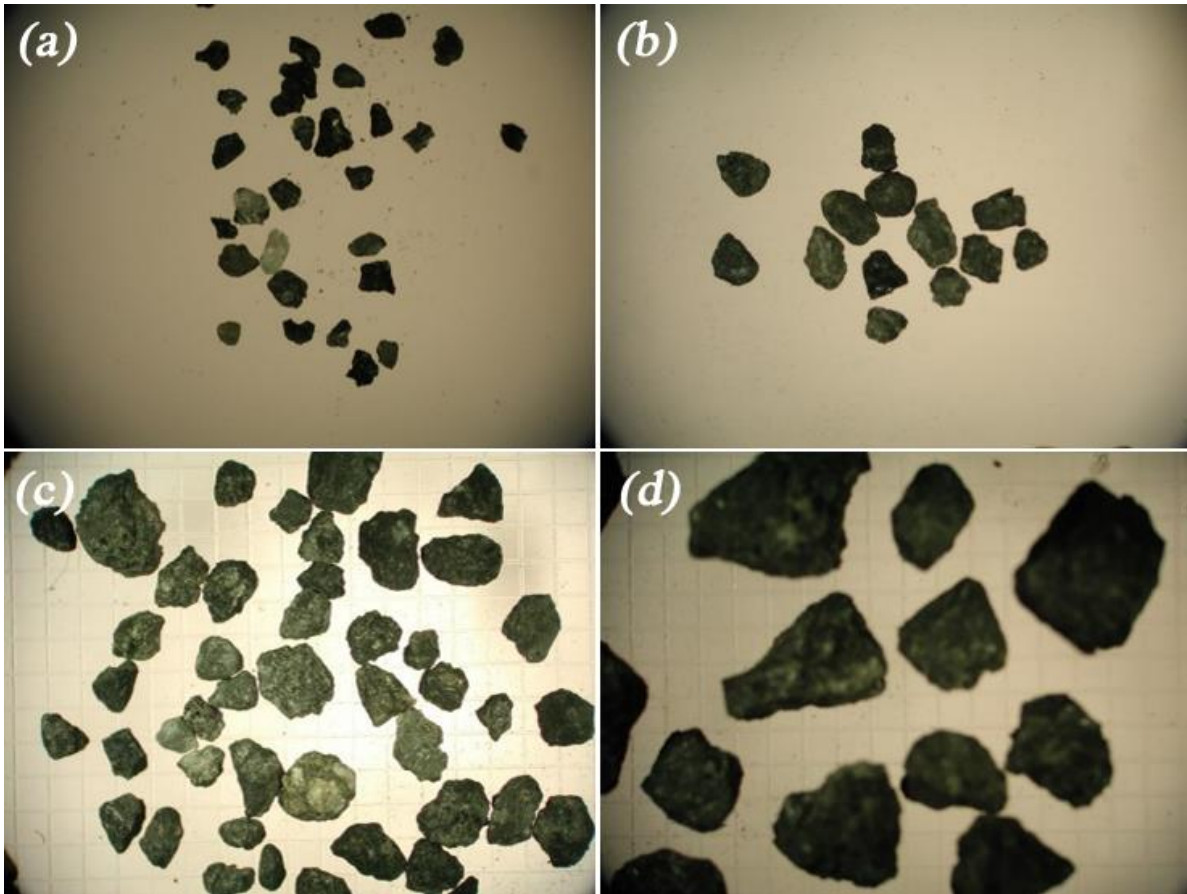
747

748

749

750

Figure 3. The locations of tephrometers and Showa crater on Sakurajima volcano, Japan. Black symbols indicate the locations of tephrometers and the star, square, and circle symbols correspond to datasets A, B and C–E, respectively. The white circle symbol represents the location of Showa crater.



751

752

753

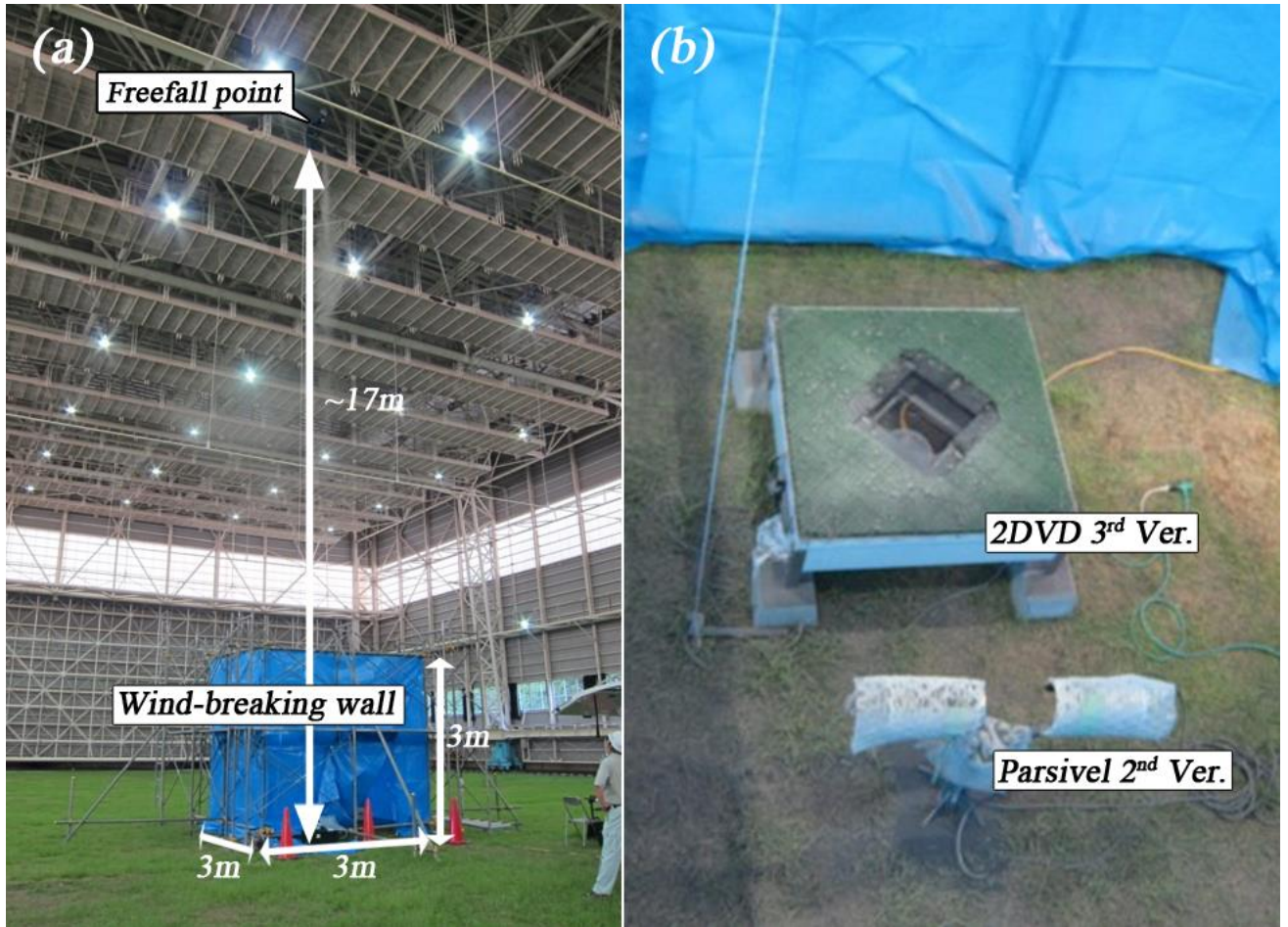
754

755

756

757

Figure 4. Real images of volcanic ash particles used in the present study. The particles were classified as (a) $0.125 \text{ mm} < D \leq 0.25 \text{ mm}$, (b) $0.25 \text{ mm} < D \leq 1 \text{ mm}$, (c) $1 \text{ mm} < D < 2 \text{ mm}$, and (d) $2 < D \leq 4 \text{ mm}$.



758

759

760

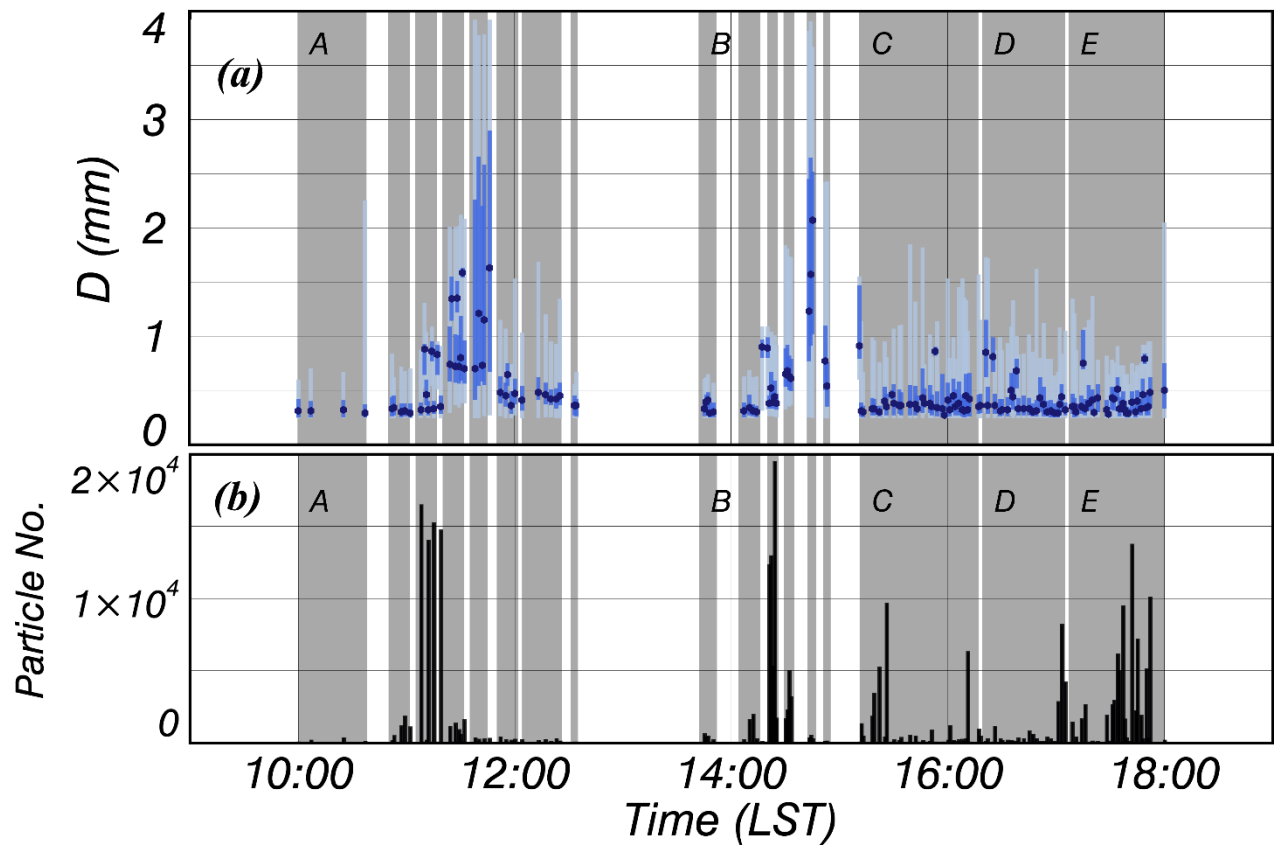
761

762

763

764

Figure 5. Free-fall experiment conditions of volcanic ash particles on the (a) outside and (b) inside of the wind-breaking wall covering the disdrometers in the large-scale rainfall simulator of the National Research Institute for Earth Science and Disaster Prevention (NIED).



765

766

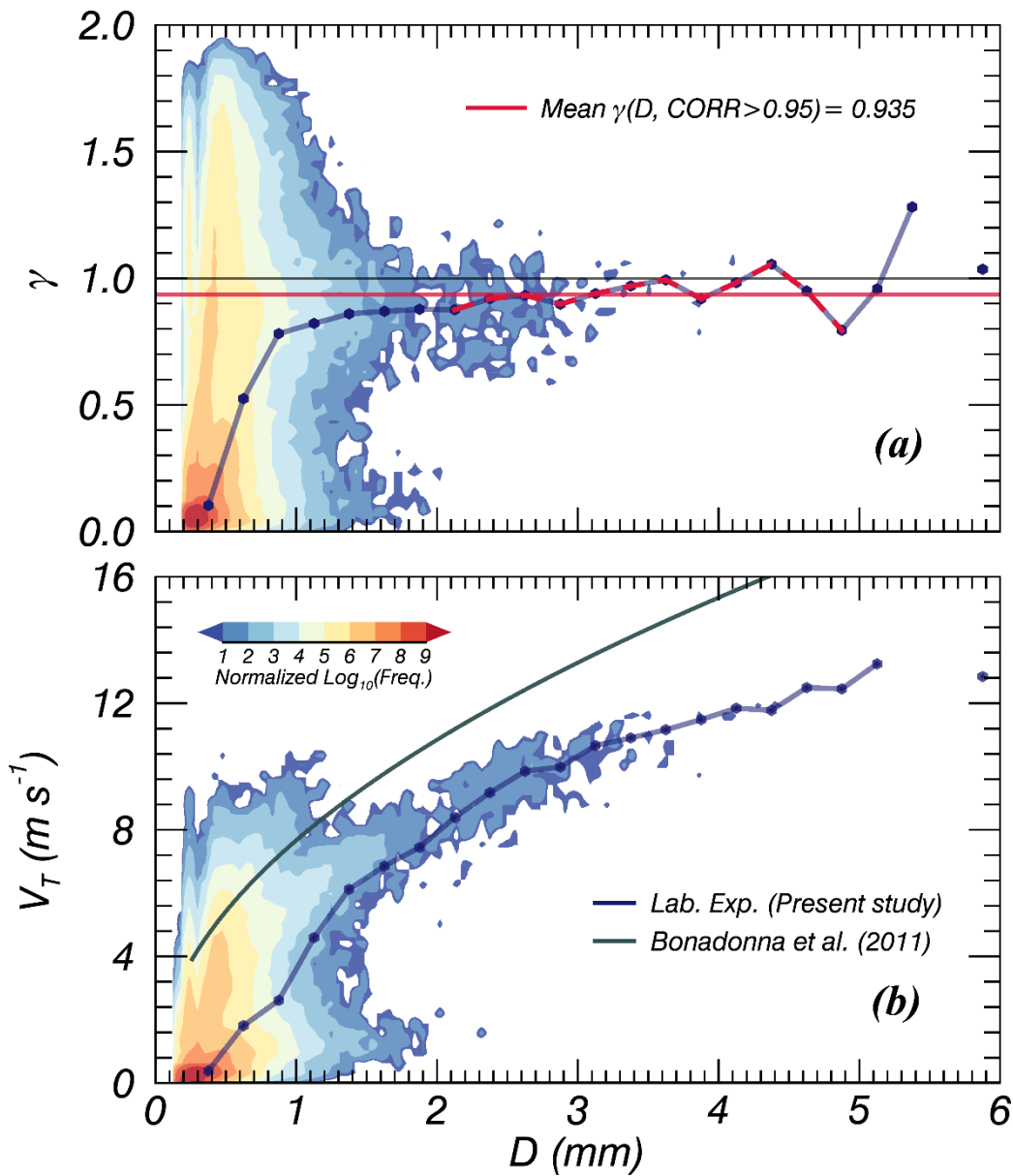
767

768

769

770

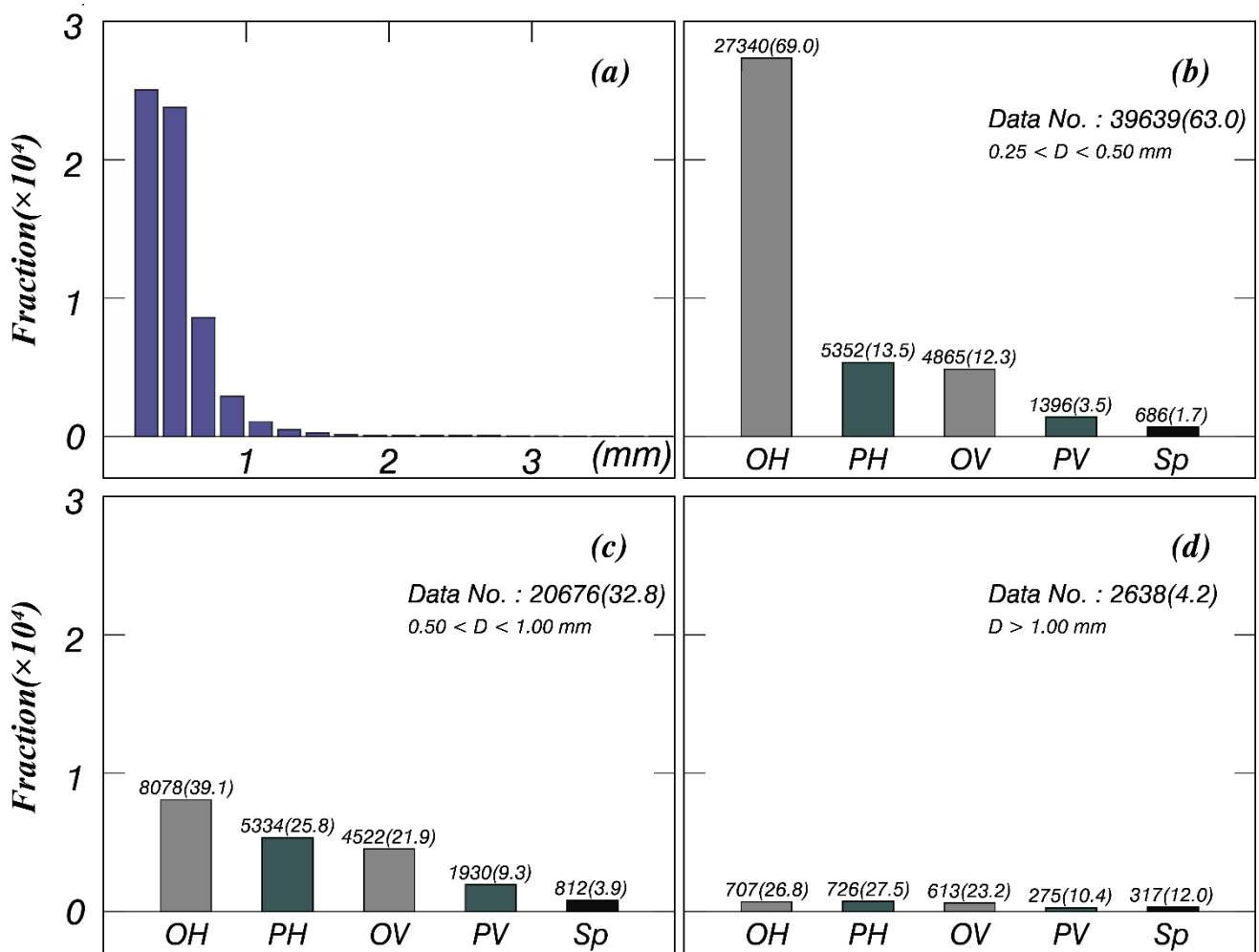
Figure 6. The 1-min interval time series of D and the number of particles in the free-fall experiment conducted at the NIED.



771

772 Figure 7. Contour image of volcanic ash particles for (a) the axis ratio (γ) and (b) terminal velocity
 773 (V_T) with respect to the sample. The red solid line is the averaged γ satisfying the condition that the
 774 correlation coefficient exceeds 0.95. Grey solid line is the relationship of volcanic ash particles
 775 suggested by Bonadonna et al. (2011).

776



777

778

779

780

781

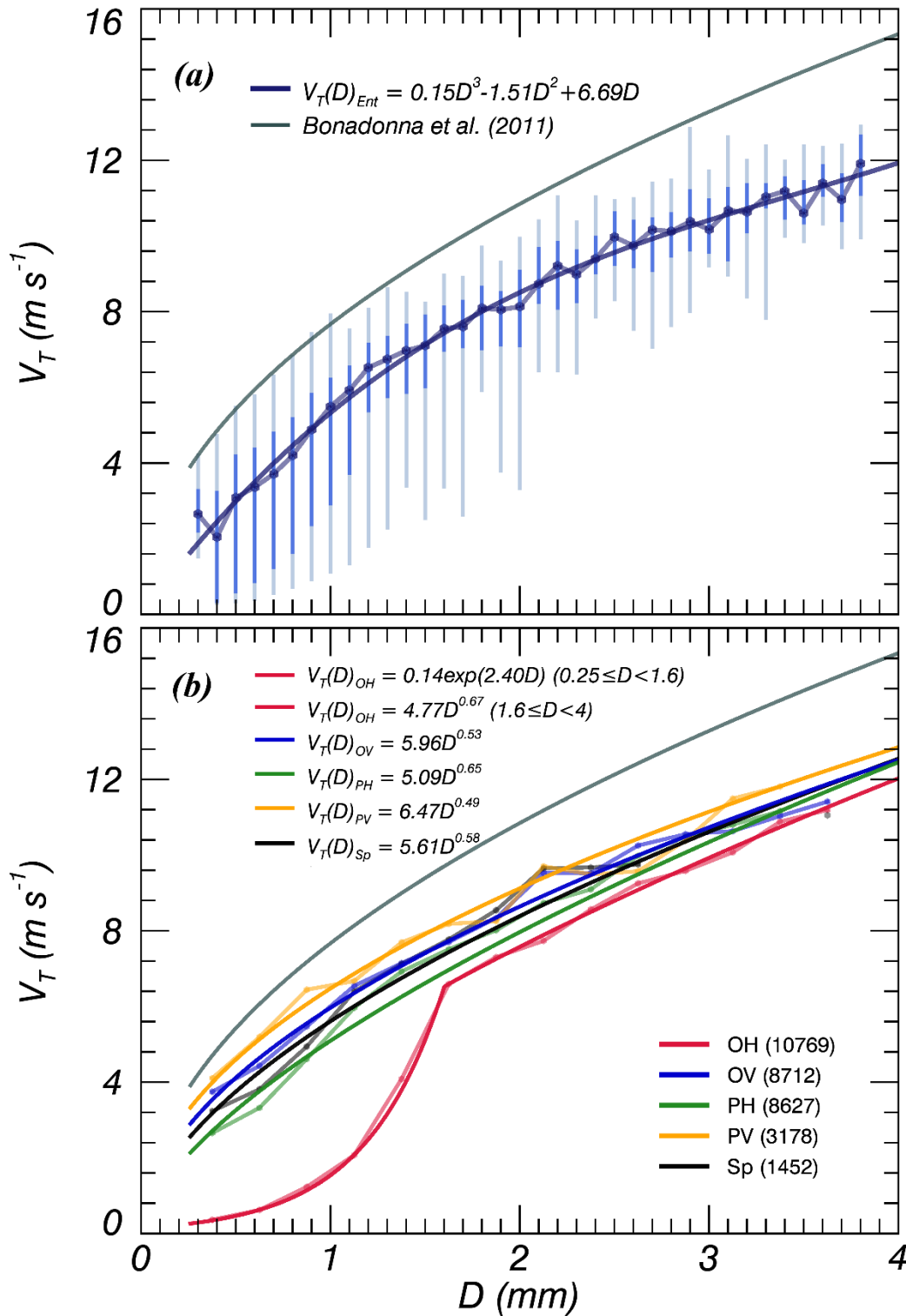
782

783

784

785

Figure 8. Histograms of volcanic ash particles for (a) all particle types and (b–d) each particle shape type of the phi scale. The grey- and dark grey-shaded (patterned) bars indicate horizontal oblate (OH) (vertical oblate [OV]) and horizontal prolate (PH) (vertical prolate [PV]), respectively. The black bar corresponds to spherical (Sp) particles. The number on the top of each bar plot is the number of data points and that in parenthesis is the percentage for each phi scale.



786

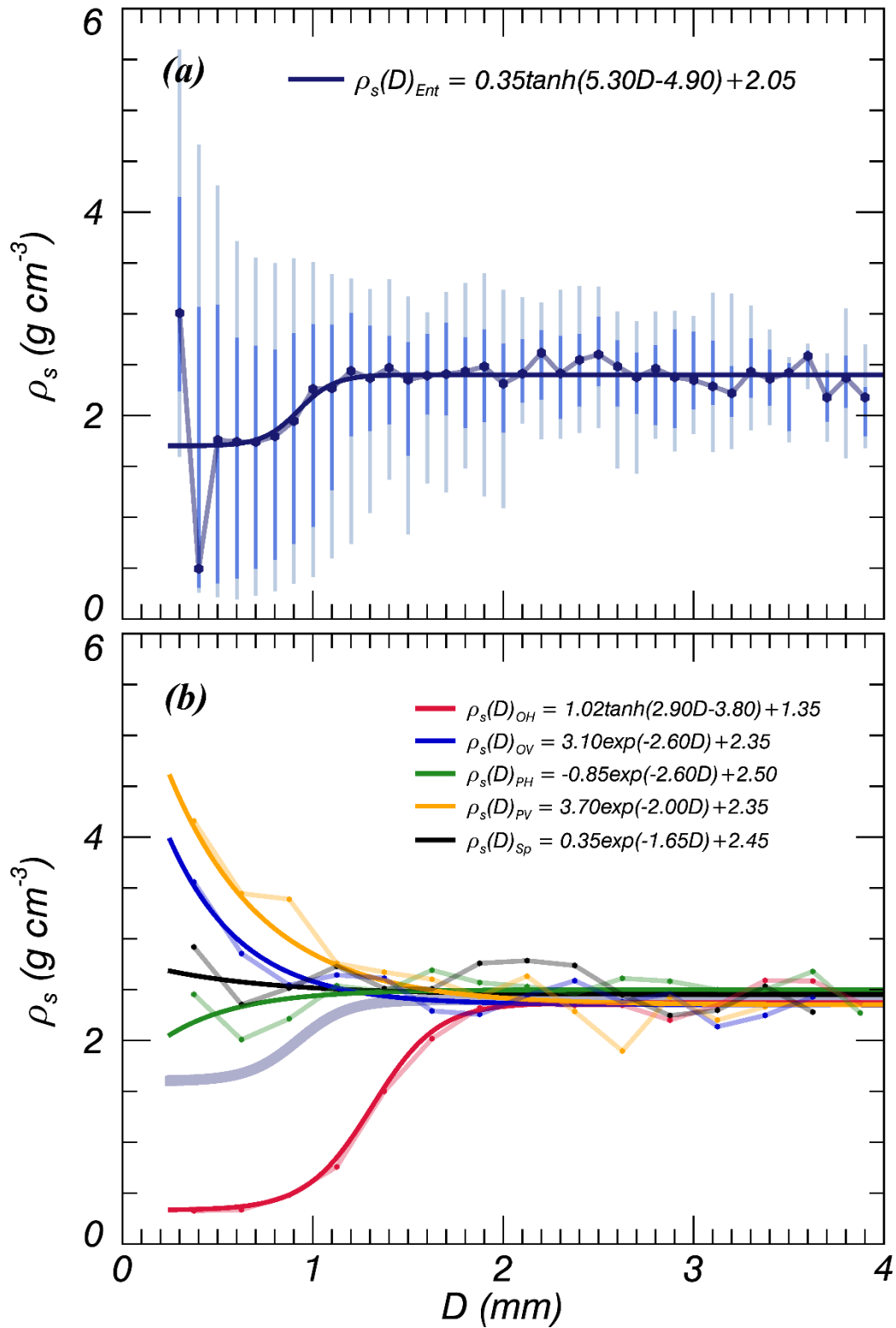
787

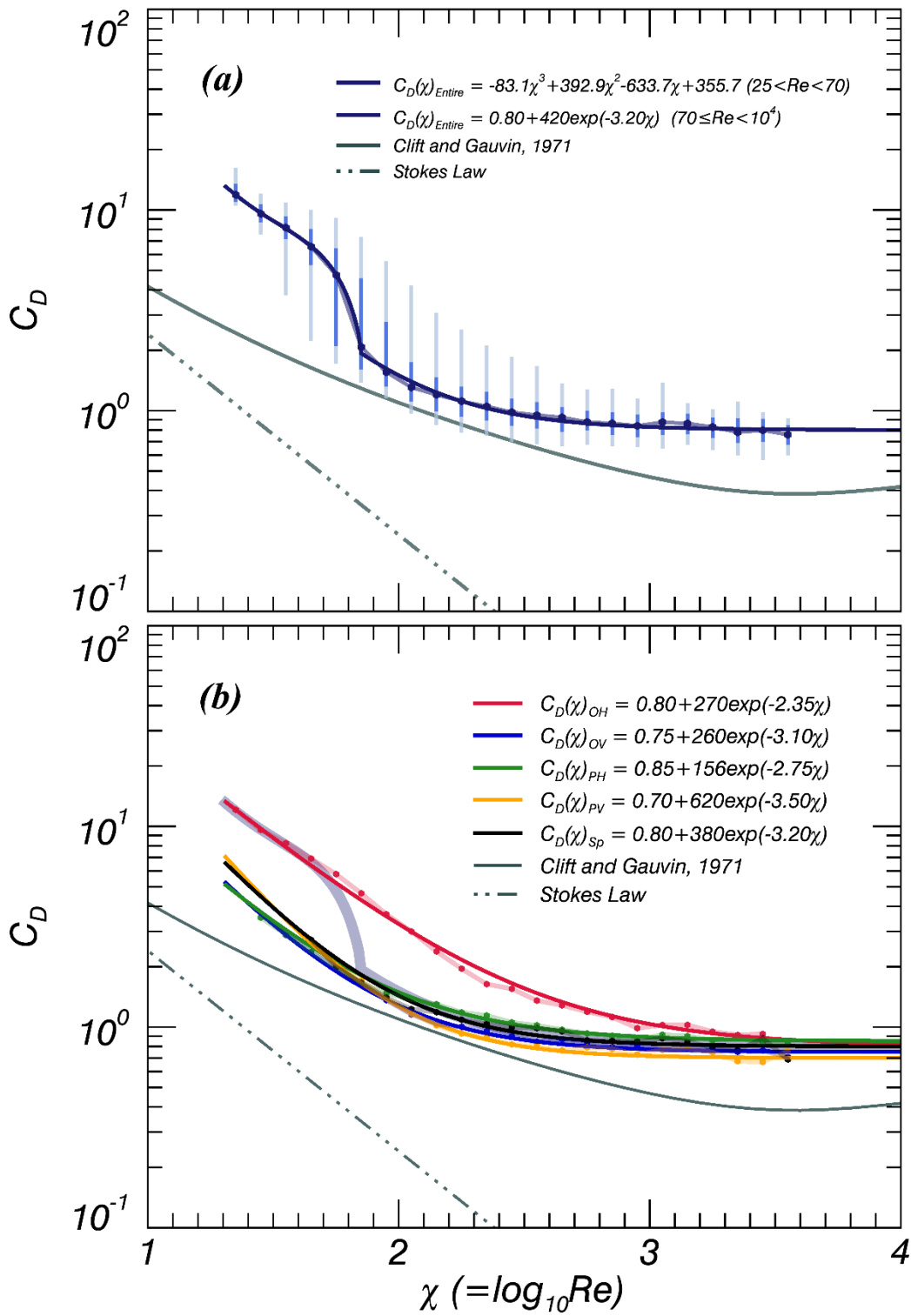
788

789

790

Figure 9. Distribution of (a) quartile and (b) median terminal velocity (V_T) values after applying the 60% V_T QC threshold for all and each individual particle shape type, respectively. The grey solid line shows the relationship of volcanic ash particles suggested by Bonadonna et al. (2011).

Figure 10. Same as Fig. 9 but for particle density (ρ_s).



795

796

797

798

799

Figure 11. Same as Fig. 9 but for Reynolds number (Re) and drag coefficient (C_D). The grey solid and broken lines in (a) are the relationships of spheres suggested by Clift and Gauvin (1971) and Stokes (1851), respectively.

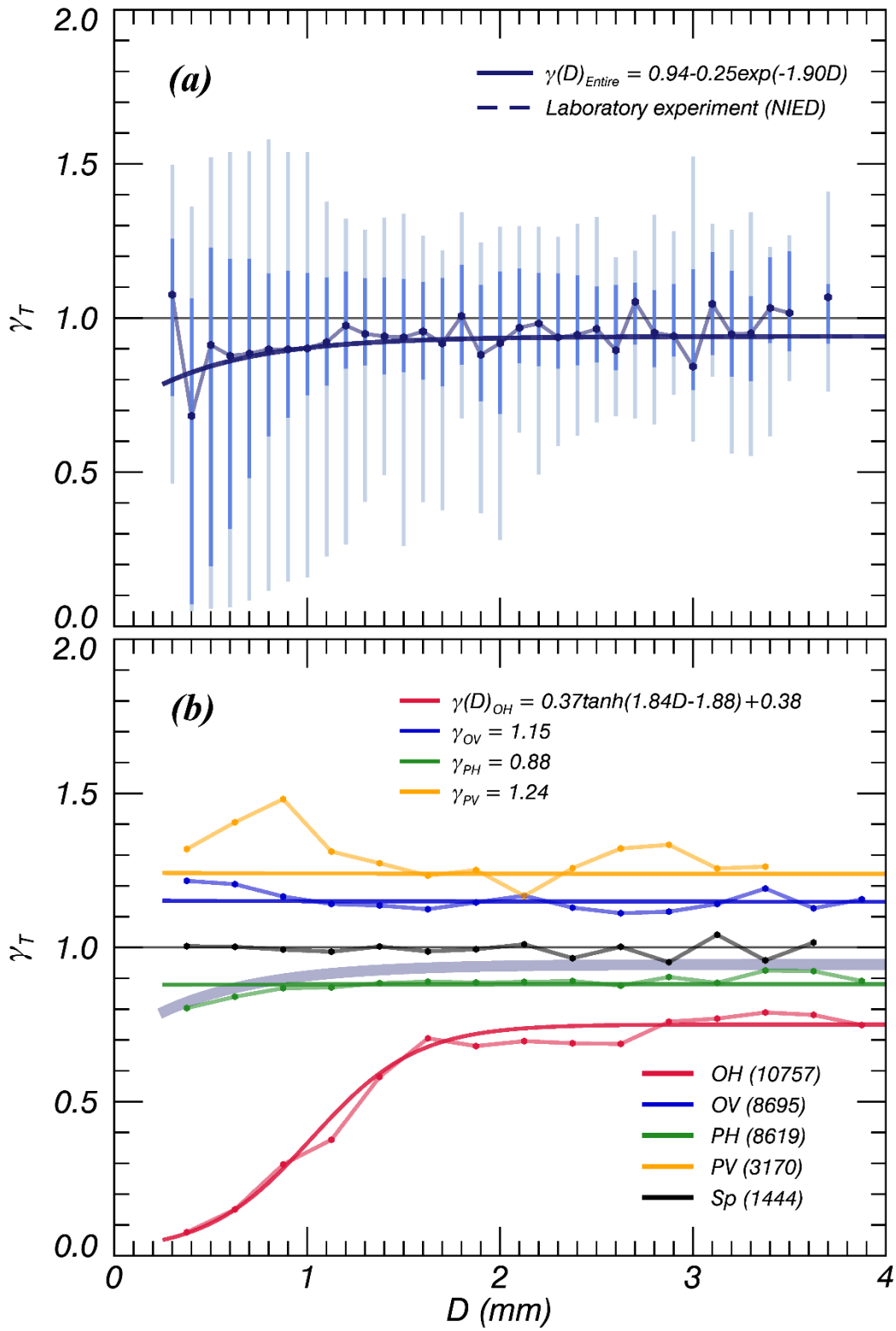
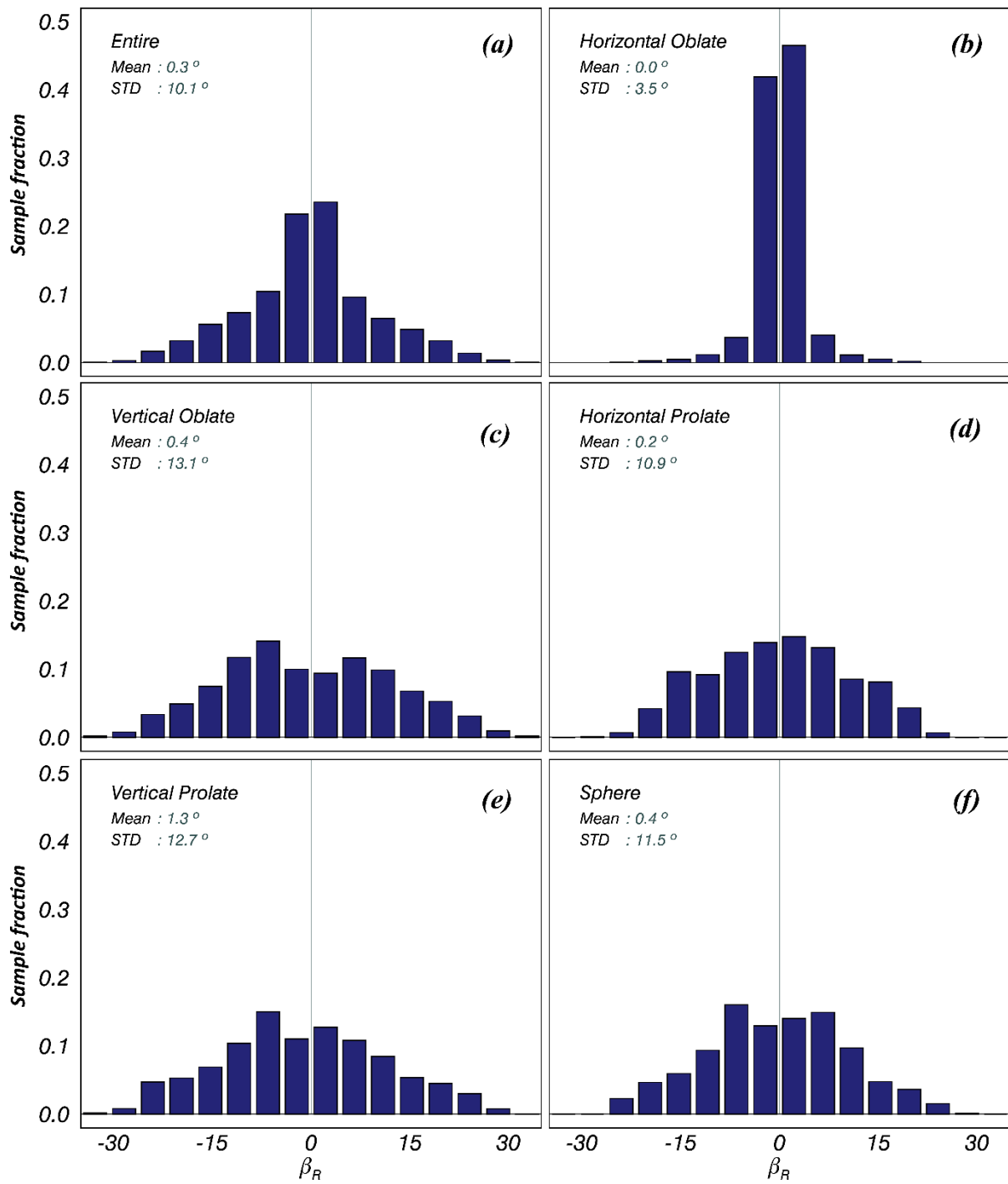


Figure 12. Same as Fig. 9 but for γ .

800
 801
 802



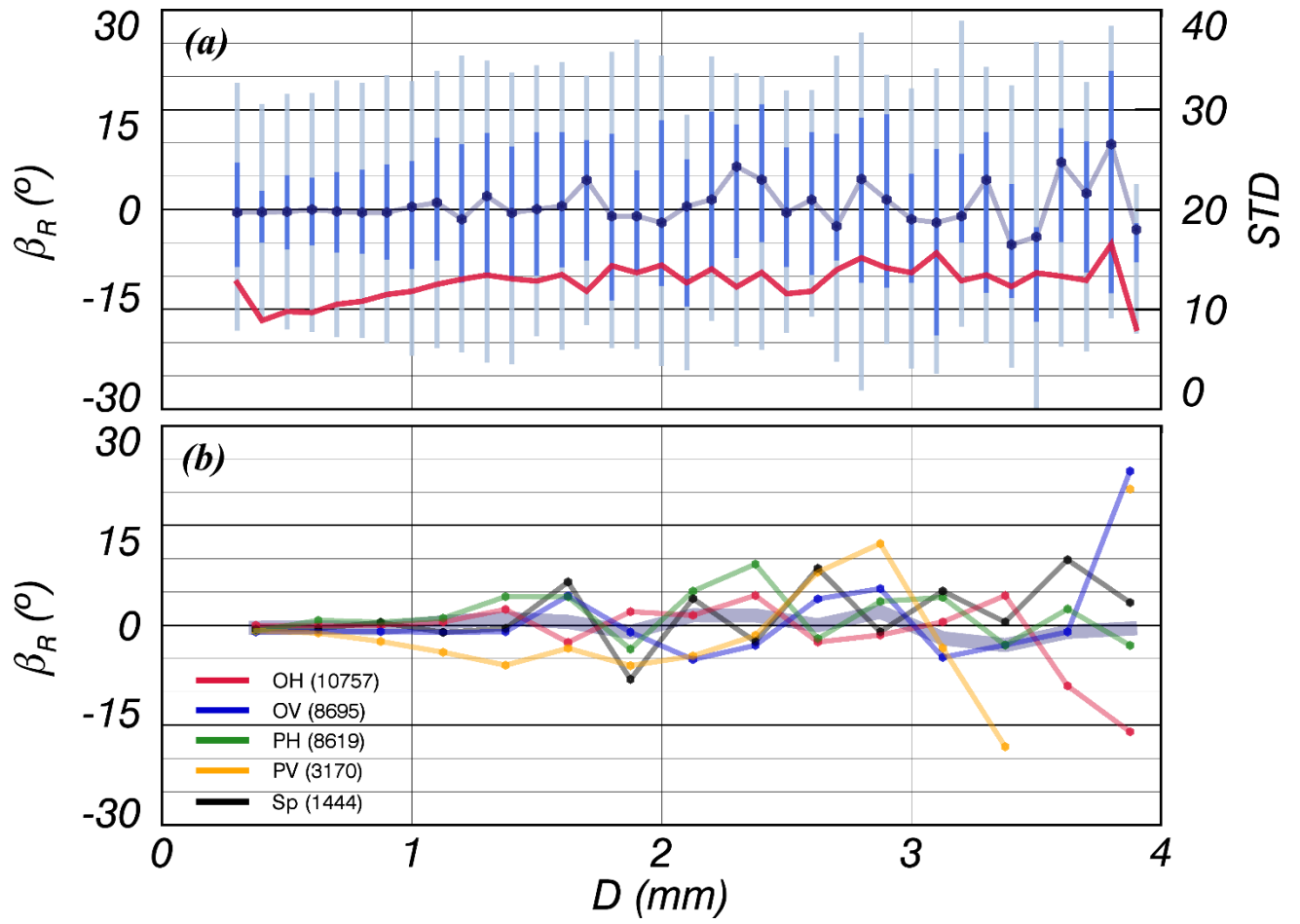
803

804

805

806

Figure 13. Histograms of representative canting angle (β_R) for each particle shape type, including the data for all particles.



807

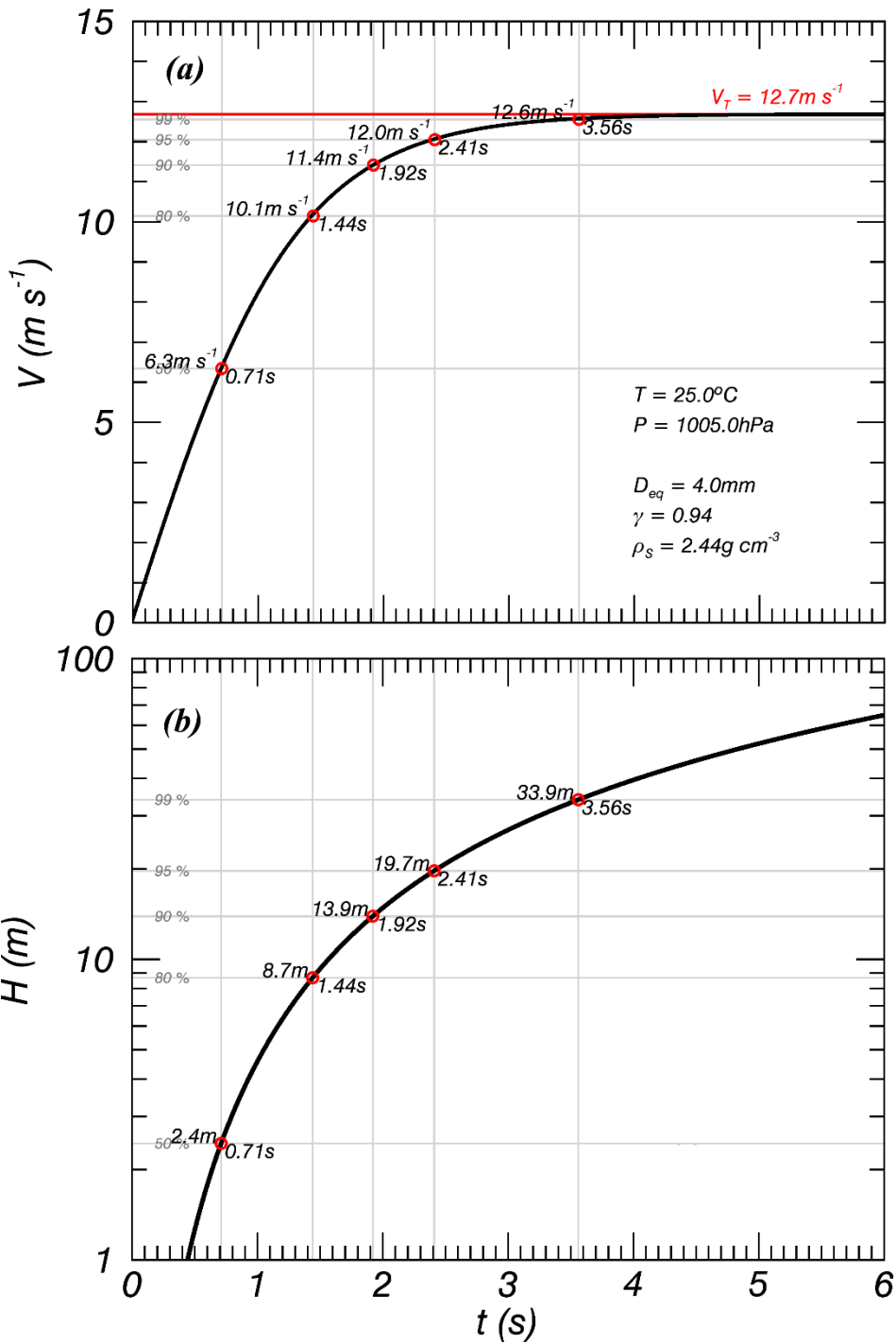
808 Figure 14. Distribution of β_R with D for each particle shape type including the data for all particles.

809 The red solid line indicates the standard deviation.

810

811

812



813

814 Figure A1. Theoretical (a) fall velocity and (b) falling height for a spheroid with $D = 4 \text{ mm}$,

815 considering the surface roughness coefficient of the volcanic ash particle (1.07^{-1}) relative to its fall

816 velocity (Bagheri and Bonadonna, 2016).

817

818 **Tables**

819

820 Table 1. Ash particle classification criteria.

Type	Description	Classification conditions
OH	Horizontal oblate	$\gamma_{T_{1(2)}} < 0.9$ $ \gamma_{T_1} - \gamma_{T_2} \leq 0.1\gamma_T$
OV	Vertical oblate	$0.9 \leq \gamma_{T_{1(2)}} \leq 1.1,$ $\gamma_{T_{2(1)}} > 1.1$
PH	Horizontal prolate	$ \gamma_{T_1} - \gamma_{T_2} > 0.1\gamma_T$
PV	Vertical prolate	$\gamma_{T_{1(2)}} > 1.1$ $ \gamma_{T_1} - \gamma_{T_2} \leq 0.1\gamma_T$
Sp	Sphere	$0.9 \leq \gamma_{T_{1(2)}} \leq 1.1$ $ \gamma_{T_1} - \gamma_{T_2} \leq 0.1\gamma_T$

821

822 Table 2. Information on the collected volcanic ash particles.

Data	Collection date	Period of free fall experiment (June 18, 2014)	Condition of free fall
A	Dec. 1–31 2008	10:00–12:34 (154 min)	Size by size (phi scale)
B	Mar. 1–31 2010	13:43–14:53 (70 min)	Size by size (phi scale)
C	Feb. 28, 2014	15:11–16:17 (66 min)	Mixed
D	Mar. 31, 2014	16:19–17:05 (46 min)	Mixed
E	Apr. 30 2014	17:07–18:00 (53 min)	Mixed

823

824

825 Table 3. Relationships of terminal velocity with the number of data points, the value of the
 826 correlation coefficient (CC) and the root mean square error (RMSE) after applying the 60% V_T QC
 827 threshold for each particle shape type.

Type	Data number (%)	Relationship ($0.25 < D \text{ (mm)} \leq 4$)	CC	RMSE
All	32685 (100)	$V_T(D) = 0.15D^3 - 1.51D^2 + 6.69D$	0.56	1.22
OH	10757 (33)	$V_T(D) = 0.14\exp(2.40D)$ ($0.25 \leq D < 1.6$)	0.94	0.46
		$V_T(D) = 4.77D^{0.67}$ ($1.6 \leq D < 4$)		
OV	8695 (27)	$V_T(D) = 5.96D^{0.53}$	0.75	0.85
PH	8619 (26)	$V_T(D) = 5.09D^{0.65}$	0.87	0.74
PV	3170 (10)	$V_T(D) = 6.47D^{0.49}$	0.71	0.96
Sp	1444 (4)	$V_T(D) = 5.61D^{0.56}$	0.91	0.78

828